



# Effect of different reinforcements in wire electric discharge machining of various geometrical profiles in metal matrix composites

Dhirendra Pratap Singh<sup>1</sup> · Sanjay Mishra<sup>1</sup>

Received: 25 October 2022 / Accepted: 30 July 2023 / Published online: 21 August 2023  
© The Author(s), under exclusive licence to Springer-Verlag France SAS, part of Springer Nature 2023

## Abstract

In this study three different geometrical profiles with same perimeter were fabricated in aluminum metal matrix composite (AMMCs) using wire electric discharge machining (WEDM). AMMCs containing Al6061 as matrix and 10% alumina ( $\text{Al}_2\text{O}_3$ ), 10% silicon carbide (SiC) and mixture of 5%  $\text{Al}_2\text{O}_3$  and 5% SiC as reinforcements were fabricated by stir casting method. The basic objective of this study is to develop response surface methodology (RSM) based second order regression model to analyze the effect of various input parameters on cutting velocity (CV) and surface roughness (SR) during WEDM of triangular, circular, and square profiles of same perimeter. Effect of pulse-on time ( $T_{\text{on}} = 30\text{--}50 \mu\text{s}$ ), pulse-off time ( $T_{\text{off}} = 6\text{--}12 \mu\text{s}$ ), current ( $I = 1\text{--}5 \text{ A}$ ) and geometrical profiles on CV and SR have been investigated using response surface plots. Parametric analysis reveals that increase of current from 1 to 5 A at  $T_{\text{on}} = 40 \mu\text{s}$ ,  $T_{\text{off}} = 12 \mu\text{s}$  increases the CV by 115% in all the three composites. Similarly, increase of  $T_{\text{off}}$  from 6 to 12  $\mu\text{s}$  at  $T_{\text{on}} = 40 \mu\text{s}$  and  $I = 1 \text{ A}$  reduces the SR by more than 35% in all composites. Multiobjective optimization using composite desirability (CD) approach shows that optimal results are obtained for triangular profiles and at optimal input parameters SR reduces by 21%, 24.19% and 33.39% respectively for alumina, silicon carbide and hybrid composite. Energy dispersive spectroscopy (EDS) analysis and SEM analysis were carried out to investigate the variation in elemental composition and surface morphology of machined surfaces respectively.

**Keywords** Wire-EDM · Cutting velocity · Surface roughness · Regression modelling · Optimization · Composite desirability · EDS · SEM · Aluminum-based metal matrix composites · Hybrid composite

## Abbreviations

WEDM	Wire electric discharge machine
AMMC	Aluminum metal matrix composite
ANOVA	Analysis of variance
MRR	Material removal rate
GRA	Grey relational analysis
TOPSIS	Technique for order of preference by similarity to ideal solution
BBD	Box–Behken design
RSM	Response surface method
SEM	Scanning electron microscopy

## 1 Introduction

Specific needs of certain niche industries, such as aerospace and automotive, led to the development of tailored made materials possessing high specific strength and rigidity. Tailorability is the main advantage of composites, and they can be fabricated to fulfill requirements that no other traditional material can achieve. Metal Matrix Composites (MMCs) are normally prepared by mixing reinforcement having superior mechanical properties with a light-weight metal matrix like Aluminium, Magnesium, Titanium etc. [1, 2]. Even though reinforcement is soluble in the matrix phase, strong adhesion exists at their interface. This results in a combined property that can't be achieved individually [3]. Composites have higher strength and low density, a high stiffness-to-weight ratio, and a high strength-to-weight ratio compared to traditional materials like steel, aluminum, etc. Aluminum metal matrix reinforced with silicon carbide (SiC) or alumina ( $\text{Al}_2\text{O}_3$ ) has high wear resistance, good fatigue and toughness, good creep resistance, and anticorrosion resistance at

✉ Sanjay Mishra  
smme@mmmut.ac.in

<sup>1</sup> Mechanical Engineering Department, Madan Mohan Malaviya University of Technology, Gorakhpur, Uttar Pradesh, India

a higher temperature. Due to their wear resistance at higher temperatures, aluminum-based metal matrix composites are mostly used in aerospace parts [4]. Conventional machining methods cannot be effectively used to create profiles in AMMC. Due to its heterogeneous character MMCs are considered to be difficult-to-cut materials because it offer considerable obstacles to the machining process. Abrasive particles with a hardness comparable to that of tools have the potential to cause significant tool wear as well as degradation in the machined surface finish. As a result, more widespread applications have been hampered by the challenges that are inherent to the machining process [5]. Electrothermal machining processes like electric discharge machine (EDM) or WEDM are generally used to cut these materials. WEDM works on the principle of EDM with a thin wire as a tool electrode. It can be used to cut electrically conductive hard and brittle materials with a high melting point. In WEDM, during pulse time, it melts the materials due to its high energy density. During pulse-off time, the flushing of deionized water on the melted surface removes the materials [6].

Many researchers have conducted experimental analysis to evaluate the performance of WEDM. Effect of servo feed (SF), pulse on time, servo voltage (SV), pulse off time, and peak current on output responses such as cutting rate, recast layer thickness, MRR, tool wear rate, kerf width, and SR have been investigated [7, 8]. Response Surface Method (RSM)-based experimental model to establish correlation between the input and output responses has been developed for better understanding of the process behavior. In order to identify significant process variables during machining, design of experiment (DoE)-based ANOVA techniques have been used by authors [8, 9]. To optimize input parameters, many techniques were used by researchers, such as multi-criterion decision making (MCDM), TOPSIS, and GRA-TOPSIS [10–12].

Hybrid MMC (HMMC) obtained by mixing two or more reinforcements in the matrix phase further improves the mechanical properties of materials [13]. Due to their unique properties, such MMCs are widely used for components of aircraft, fighter planes, and automobile components. HMMCs reinforced with graphite have a lower friction coefficient, whereas composites reinforced with SiC have a lower wear rate [14]. It was found that mixing of SiC as reinforcement improves the tensile strength, stiffness, and friction, whereas mixing of  $Al_2O_3$  enhances the hardness and compressive strength of the parent material [15, 16]. Kumar et al. [17] developed a hybrid AMMC by reinforcing SiC, Graphite and ferrous oxide and investigated it on WEDM for MRR, SR, and SG (Spark Gap), optimised the response by AHP (Analytical Hierarchy Process) and GA (Genetic Algorithm), and achieved the best machining conditions at pulse current ( $I_p$ ) at 80 A, pulse on time ( $T_{on}$ ) at 0.5  $\mu$ s, pulse of time ( $T_{off}$ ) at 12  $\mu$ s, WF (Wire Feed) at 5 m/min, WT (Wire Tension)

at 850 G, and SV at 35 V. Lal et al. [18] developed a hybrid AMMC by mixing 7.5%  $Al_2O_3$  and 7.5% SiC in Al7075 through a stir casting process and did his investigation on WEDM, and from ANOVA, the order of significance of input parameters and contribution to responses was as follows:  $T_{on}$  was 50.02%, I was 39.50%,  $T_{off}$  was 4.58%, and WS (wire speed) was 2.75%. Raju et al. [19] found optimised input parameters for AMMC reinforced with silicon nitride were  $T_{on}$  of 130  $\mu$ s, current of 20 A, and wire feed of 1 mm/min for higher MRR on WEDM. It was found that  $T_{on}$  and I have a direct influence on MRR and SR [20, 21]. Khanna et al. [22] develop a hybrid composite using SiC and Ti reinforced by stir casting. And use a hybrid optimisation process as RSM-ARAS-TLBO algorithm, in which BBD approach of RSM was used to experimental design, further response variables were converted into optimality function using Additive Ratio Assessment (ARAS), and then the developed empirical model was solved by teaching learning based optimization (TLBO). And they found that the optimised input parameters for WEDM were  $T_{on}$  at 128  $\mu$ s;  $T_{off}$  at 48  $\mu$ s; SV at 48 V, and WF at 7 m/min. The finished surface of the workpiece that was cut by WEDM has a lower SR as compared to conventional machining [23]. Pramanik et al. [24] found that when reinforced particles were smaller in size, there was more surface defect in the machining surface, and circularity error could be improved by mixing medium-sized reinforcement. Due to the increasing pulse on time and the higher energy density, it melts the material, and there is more time to degrade the cut surface of WEDM machining. Then low pulse on time and wire tension give high-quality SR [25]. Authors have reported that discharge current and pulse on or off time were the most influential parameters on MRR and SR as compared to open circuit voltage [26, 27].

Joy et al. [28] conducted angular cutting at angles of 0°, 30°, and 60° using WEDM to eliminate the disadvantage of taper cutting WEDM. And they perform his experiment using the Taguchi  $L_9$  experimental design for cutting speed, recast layer thickness, and SR. Nayak et al. [29] optimized process parameters using a utility concept approach for taper cutting on WEDM by considering input parameters such as part thickness, taper angle, pulse duration, discharge current, wire speed, and wire tension at three levels for obtaining responses like angular error, surface roughness, and cutting speed. Manoj et al. [30] cut three shapes, a triangle, a square, and a circle, at two different angles of 0° and 30° in three different sizes, 1, 3, and 5 mm, which were machined at WEDM. And found that the cutting speed override parameter affected the profiling speed the most in both angles, irrespective of profiles. And they did another experiment machining Altemp HX on WEDM by considering  $T_{on}$ , wire span, and SV as input parameters to examine the CV, SR, Recast layer, and microhardness WEDMed surface. And optimized CV and SR by Genetic algorithm and compared the output predicted

by the RSM and ANFIS models. And conclude that ANN has a 6% lesser error as compared to RSM [31]. Selvakumar et al. [32] enhanced the die corner accuracy with a trim cut in WEDM for Monel 400 alloy. Devarajaiah et al. [33] evaluate power consumption and MRR for Ti–6Al–4 V on WEDM by considering pulse on time (13, 20, 27, 34  $\mu$ s), pulse off time (4, 6, 8, 10  $\mu$ s), applied current (1, 2, 4, 5 A), and wire speed (WS 350, 700, 1050, 1400 rpm) for sustainable production. And experimental inquiry reveals that I and  $T_{off}$  are key influencing variables for MRR and PC. Surface plots are used to study the parametric variation of the MRR and PC response surfaces.

Ilani et al. [34] conducted their experiment using a copper-coated acrylonitrile butadiene styrene electrode. Rapid prototyping by fused deposition modeling was utilized to increase the conductivity of electrode tools. This powder-mixed EDM has a significant impact on manufacturing time and surface quality. In their other studies, they take I,  $T_{on}$ , and the concentration of added aluminum powder as input parameters. In their experiment, they found that adding aluminum powder reduced kerosene's dielectric resistance. Additionally, their mathematical and physical models showed that the addition of powder had a beneficial impact up to 2.5 g/l [35]. According to Taherkhani et al. [36], the micron-sized  $Al_2O_3$  powders may greatly improve the surface quality of the Ti–6Al–4 V during the PMEDM process of machining. It is quite challenging to uniformly distribute powder particles into the plasma channel. So surfactant Tween 80<sup>®</sup> was put in EDM oil, which affects intermolecular forces (IMF) via the plasma channel and improves surface quality evaluation [37]. As a result of the formation of  $TiO_2$  (Titanium dioxide) on the experimental surface, the corrosion resistance, biocompatibility, and biofunctionality of Ti–6Al–4 V are enhanced [38]. TWR of coated and uncoated electrodes in EDM for Ti–6Al–4 V titanium alloy was compared by Phan et al.; Aluminum serves as the primary electrode material, while AlCrNi works as the surface coating. Taguchi approach was used to survey process parameters such as current (I), gap volt (V), and pulse on time ( $T_{on}$ ). The findings demonstrated that  $T_{on}$  and I had a significant impact on both electrodes TWR (tool wear rate) and MRR. The TWR of an Al electrode is around 24% greater than that of an Al electrode that has been coated [39, 40]. Studies on EDM have shown that selecting the right method for controlling the process, material, and operating parameters significantly enhanced the process performance and also led to a better-quality machined surface [41].

Boopathi [42] performed his experiment on near-dry WEDM, in which he used pressurised air with a small amount of water as the dielectric. Because in conventional WEDM, the dielectric used affects the environment, The Taguchi analysis was used to improve the effects of machining parameters (air pressure, flow rate mixing water, spark current, and

pulse width) on gas emission concentration (GEC), material removal rate (MRR), and relative emission rate (RER) of a near-dry WEDM process. Gowri et al. [43] use oxygen-mixed dielectric fluid for near-dry EDM and perform experiments on shape memory alloys with a copper composite electrode. And found that TWR significantly decreased in near-dry EDM. The author also investigates the machining properties using compressed air combined with a small amount of biodegradable refined sunflower oil (called oil mist) [44]. Xie et al. [45] did their experiment on near-dry WEDM for cutting die steel. They used a novel dielectric fluid feeding method, the moistened wire method, for near-dry WEDM. For which a dielectric was poured on the wire drum to achieve moistened wire. And use gas–liquid double-layer dielectric for discharge machining, cooling, and cleaning the work-piece material. They found that moistened wire improved the machined surface quality and corner accuracy of cutting.

The above literature survey reveals that several studies related to parametric analysis and optimization of WEDM process to improve the machinability of AMMCs have been reported. But very few work related to the modelling and multiobjective optimization of CV and SR for WEDM of different geometrical shapes possessing same perimeter in AMMCs of different composition have been reported. In this study, AMMCs of three different compositions containing (i) 10 wt% alumina (ii) 10 wt% SiC and (iii) 5 wt% alumina and 5 wt% SiC have been prepared by the stir casting method. The BBD approach of RSM has been used to develop a second-order regression model for each output parameter to analyze the effect of input factors like  $T_{on}$ ,  $T_{off}$ , I, and shape on CV and SR. Furthermore, the optimal input parameters were also obtained using the composite desirability approach of RSM. EDS and SEM analysis of the WEDMed surface at optimal and non-optimal input parameters were also conducted to establish the efficacy of optimal parameters.

## 2 Materials and method

### 2.1 Aluminum metal matrix composites

In this work, three different MMCs using aluminum alloy (Al6061) as matrix were fabricated by stir casting method as per the details given in Table 1. Al6061 is generally used in structural and transportation applications where high tensile strength and hardness are needed. It is a preferred structural material in the maritime industry due to its excellent anti-corrosion qualities. The chemical composition and mechanical properties of Al6061 is shown in Table 2. The aluminum alloy was heated up to 800<sup>o</sup>C in an electric furnace in a graphite crucible. The preheated reinforcement was mixed in the molten metal for nearly 5 min. Preheating helps to reduce the casting's porosity by removing the moisture

**Table 1** Fabricated aluminum metal matrix composites (AMMCs)

Matrix	Reinforcements	Reinforcements wt%	Composite formed
Aluminum alloy (Al6061)	Al <sub>2</sub> O <sub>3</sub>	10	Al-6061–10% Al <sub>2</sub> O <sub>3</sub>
	SiC	10	Al-6061–10% SiC
	Al <sub>2</sub> O <sub>3</sub> + SiC	5 each	Al-6061–5% Al <sub>2</sub> O <sub>3</sub> –5% SiC

from reinforcement. Reinforcements as shown in Table 1 were mixed in the melted aluminum alloy by stir casting using four blade stirrer.

### 2.2 Experimentation

As shown in Fig. 1a experiments were performed on CNC wire cut EDM (MODEL EX-4050C) using molybdenum wire electrode of diameter 0.18 mm at the wire speed of 10.4 m/s. Since wear produced in molybdenum wire electrode is negligible during machining and it has high melting point with good tensile strength; therefore, it yields better cutting rate while producing intricate profiles during WEDM. Deionized water was used as the dielectric medium for the machining of all AMMCs. Figure 1b shows the schematic diagram of the WEDM, in which the workpiece is clamped in the workpiece holding device. A wire is moved through the top and bottom wire guides, and an automatic spring tensor is used to maintain the wire tension. Since it is a high-voltage, low-current process; therefore, initially the deionized water is non-conducting, but once voltage is applied, it turns into conducting medium in a narrow zone. Current flow in the circuit when the voltage discharges from its threshold value. When there is a minimum gap between the workpiece and wire, sparks are produced, due to which material get melt and removed from the surface during pulse-off time.

**Table 2** Compositions and mechanical properties of Al6061 [46]

S. no.	Composition		Mechanical Properties at room temperature	
	Element	Wt%		
1	Al	Balance	Poisson’s ratio	0.33
2	Mg	1.12	Thermal expansion	23.8 × 10 <sup>-6</sup> /K
3	Mn	0.01	Melting point (°C)	650
4	Cu	0.33	Density (g/cc)	2.7
5	Cr	0.05	Thermal conductivity (W/m K)	166
6	Si	0.71	Strength (MPa)	180
7	Fe	0.17	Modulus of elasticity (GPa)	70

Initially, a pilot experiment was conducted to find the level of input parameters. Each experiment was repeated thrice to reduce the effect of high variability or uncertainties. The input parameters with their levels as shown in Table 3 has been selected based on significance of their effect on output parameters i.e. cutting velocity (CV) and surface Roughness (SR). As shown in Fig. 2 triangular (T), circular (C) and square (S) profiles possessing same perimeter were produced on the prepared composite of 5 mm thickness. Table 4 shows the experimental design for the WEDM of Al6061–10% SiC, Al6061–10% Al<sub>2</sub>O<sub>3</sub>, and Al6061–5% Al<sub>2</sub>O<sub>3</sub>–5% SiC AMMCs.

In this study, Eq. 1 was used to evaluate the CV. In WEDM process the value of CV can be used to predict the MRR as shown in Eq. 1. Thus CV represents the productivity of WEDM process. So in this experimental work we consider CV and SR as the output responses.

Since craters are produced on the machined surface during WEDM due to spark energy and high value of SR decreases the fatigue life of machined components therefore SR is a critical parameter to evaluate the machining performance. Furthermore, the value of SR also affects the primary functionality of machined components. SR of the machined surface were determined using the Taylor Hobsons Surface Roughness tester with cut off length (λ<sub>c</sub>) 0.8 mm and evaluation length 4 mm with 100 μm range. Before measuring the SR on sample a reference sample was measure with 6 μm average SR.

$$\left. \begin{aligned}
 CV &= \frac{\text{perimeter of cutting surface} \times 60}{\text{Operation Time(s)}} \\
 MRR &= CV \times \text{wire diameter} \times \text{material thickness}
 \end{aligned} \right\} \tag{1}$$

### 2.3 Response surface methodology (RSM)

It is a statistical and mathematical technique used to design the experiment based on given input parameters and their

**Fig. 1** a Wire EDM and b schematic diagram of WEDM

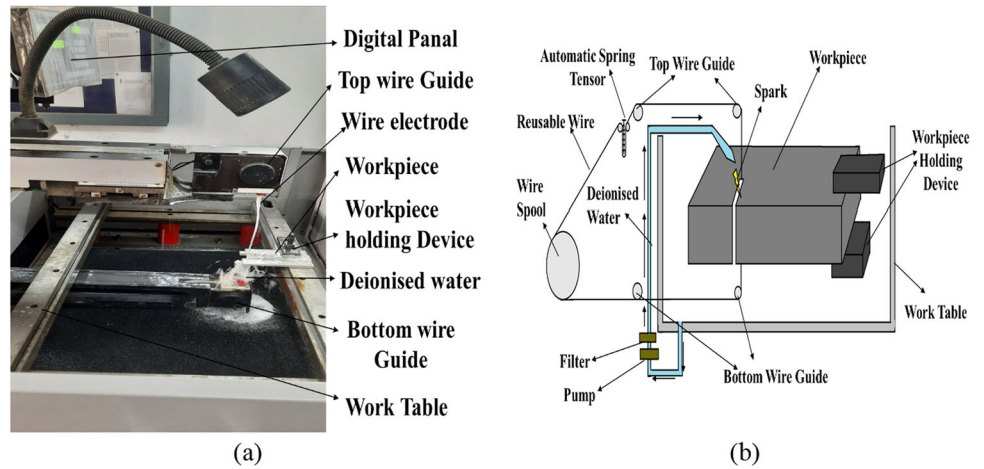


**Table 3** Process parameters and their levels

Input parameters	Symbols	Units	Levels		
			- 1	0	+ 1
Pulse-on-time	T <sub>on</sub>	μs	30	40	50
Pulse-off-time	T <sub>off</sub>	μs	6	9	12
Current	I	Ampere (A)	1	3	5
Shape	-	-	T	C	S

T triangular shape, C circular shape, S square shape



**Fig. 2** Experiment performs on WEDM

BBD approach, 2<sup>2</sup> full factorial acts as base design and then orthogonal blocks are formed using the mid-levels for the other factors. It uses face points, which is normally more practical than the corner points used in the central composite design (CCD) approach of RSM. The inclusion of the middle level point helps to effectively determine the coefficients of a second-order model. BBD approach is also rotatable like CCD and requires smaller number of experimental trails. Therefore, BBD has been used here to create second order regression model based on three-level factorial design [48]. In this experiment, machining performance CV and SR were modeled in terms of pulse-on time, pulse-off time, current, and shape of geometry produced during machining.

$$A = C_0 + \sum_{k=1}^n C_k * u_k + \sum_{k=1}^n C_{kk} * u_{kk}^2 + \sum_{k < m}^n C_{km} * u_k * u_m \tag{2}$$

level [47]. RSM is used to predict the machining performance of WEDM in terms of CV and SR with given input process parameters. The experiment were conducted based on the Box–Behnken Design (BBD) approach of RSM. In

Equation 2 shows the 2nd order regression model generated by the RSM [17], where, A is the output response and C<sub>0</sub>, C<sub>k</sub>, C<sub>kk</sub>, and C<sub>km</sub> are unknown regression coefficients, and u<sub>k</sub>, and u<sub>m</sub> are input process parameters.

**Table 4** Observation table for machining of AMMC

S. no.	T <sub>on</sub>	T <sub>off</sub>	I	Shape	Al6061–10% Al <sub>2</sub> O <sub>3</sub>		Al6061–10% SiC		Al6061–5% Al <sub>2</sub> O <sub>3</sub> –5% SiC	
					CV (mm/min)	SR (μm)	CV (mm/min)	SR (μm)	CV (mm/min)	SR (μm)
1	30	6	3	C	6.7404	5.955	6.7982	5.58	6.8275	5.4791
2	50	6	3	C	6.9170	7.2366	6.9779	8.2	7.0088	7.3324
3	30	12	3	C	6.6554	6.085	6.7404	6.1566	6.7118	5.8147
4	50	12	3	C	6.7692	6.8616	6.8275	6.9733	6.7982	6.5716
5	40	9	1	T	4.4	5.3416	4.4245	5.5766	4.4122	5.1862
6	40	9	5	T	6.8869	7.4333	7.04	7.6	6.9473	7.1408
7	40	9	1	S	4.5780	6.37	4.3878	6.2833	4.2695	6.0103
8	40	9	5	S	6.8275	6.6466	6.8275	6.8966	6.8869	6.4330
9	30	9	3	T	6.6835	6.0266	6.7692	5.48	6.8275	5.4656
10	50	9	3	T	6.8869	7.35	6.9779	8.4166	6.9473	7.4891
11	30	9	3	S	6.6	6.9416	6.6554	6.61	6.6276	6.4370
12	50	9	3	S	6.7692	7.52	6.8571	6.8466	6.8869	6.8241
13	40	6	1	C	6.2117	5.9166	6.2608	5.6533	5.9325	5.4957
14	40	12	1	C	3.2	5.6033	3.2392	5.1933	3.2392	5.1284
15	40	6	5	C	6.7692	6.8083	6.8275	6.0133	6.7982	6.0902
16	40	12	5	C	6.8571	6.4183	6.8869	5.63	6.8869	5.7229
17	30	9	1	C	4.7567	5.21	4.8	4.8566	4.5257	4.7816
18	50	9	1	C	4.95	6.3433	4.9655	6.2166	3.9305	5.966
19	30	9	5	C	7.1031	6.1666	7.2	5.45	6.8275	5.5179
20	50	9	5	C	7.04	6.7466	7.0714	6.83	6.8571	6.4489
21	40	6	3	T	6.6835	7.56	6.7982	7.2066	7.0088	7.0141
22	40	12	3	T	7.1674	6.9466	7.2	7.38	6.9473	6.8051
23	40	6	3	S	7.2	7.1683	7.2328	6.8366	7.0088	6.6523
24	40	12	3	S	7.1674	6.705	7.1031	6.1933	6.8869	6.1267
25	40	9	3	C	7.1351	6.4433	7.1674	6.16	6.8571	5.9865
26	40	9	3	C	7.0714	6.7216	7.1031	6.34	6.8275	6.2042
27	40	9	3	C	6.6554	6.935	6.7118	7.1233	6.6	6.6777

## 2.4 ANOVA

It is a statistical technique used to calculate the comparative importance of all input parameters by decomposing the variance at a particular confidence level. In this paper, ANOVA has been performed using MINITAB-18 software. An ANOVA table consists of many factors such as degree of freedom (DF), sum of the square (SS), mean square (MS), percentage contribution, *P* and *F* values. *P* value and *F*-value characterize the relative importance of input parameters. This higher *F*-value and Lower *P* value show a better contribution of input parameters to the output parameters. Since a 95% confidence level is used in this paper, the *P* value less

than 0.05 shows the significant parameters' effect on the output [49]. The following Fig. 3 show the graphical summary experimental studies and result of present work.

## 3 Results and discussion

### 3.1 RSM based regression model for CV

Equations 3, 4, and 5 as given below are the second-order regression model for CV for Al6061–10% Al<sub>2</sub>O<sub>3</sub>, Al6061–10% SiC, and Al6061–5% Al<sub>2</sub>O<sub>3</sub>–5% SiC, respectively.

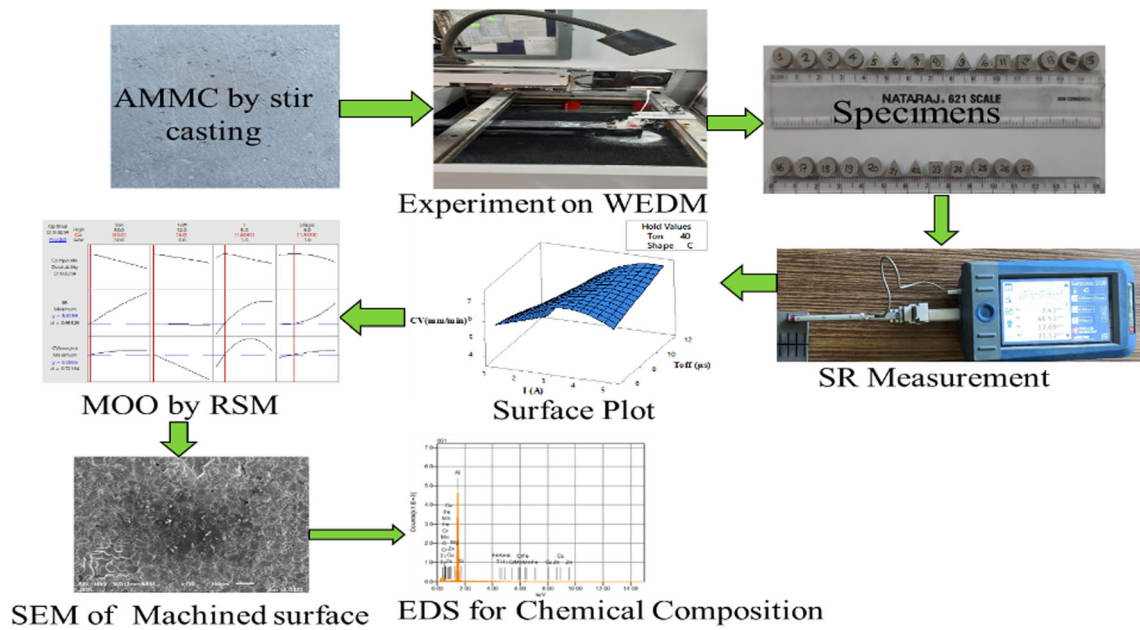


Fig. 3 Graphical summary of presented work

$$\begin{aligned}
 CV(\text{mm/min}) = & 3.54 + 0.078 T_{\text{on}} - 0.335 T_{\text{off}} + 1.241 I + 0.83 \text{ shape} - 0.00069 T_{\text{on}} * T_{\text{on}} \\
 & - 0.0012 T_{\text{off}} * T_{\text{off}} - 0.2763 I * I - 0.072 \text{ shape} * \text{shape} - 0.00052 T_{\text{on}} * T_{\text{off}} \\
 & - 0.0032 T_{\text{on}} * I - 0.0009 T_{\text{on}} * \text{shape} + 0.1292 T_{\text{off}} * I - 0.0430 T_{\text{off}} * \text{shape} \\
 & - 0.030 I * \text{shape}
 \end{aligned} \tag{3}$$

$$\begin{aligned}
 CV(\text{mm/min}) = & 4.10 + 0.053 T_{\text{on}} - 0.336 T_{\text{off}} + 1.297 I + 0.79 \text{ shape} - 0.00037 T_{\text{on}} * T_{\text{on}} \\
 & - 0.0006 T_{\text{off}} * T_{\text{off}} - 0.2813 I * I - 0.082 \text{ shape} * \text{shape} - 0.00077 T_{\text{on}} * T_{\text{off}} \\
 & - 0.0037 T_{\text{on}} * I - 0.0002 T_{\text{on}} * \text{shape} + 0.1284 T_{\text{off}} * I - 0.0443 T_{\text{off}} * \text{shape} \\
 & - 0.022 I * \text{shape}
 \end{aligned} \tag{4}$$

$$\begin{aligned}
 CV(\text{mm/min}) = & 7.99 + 0.004 T_{\text{on}} - 0.645 T_{\text{off}} + 1.032 I - 0.474 \text{ shape} - 0.00034 T_{\text{on}} * T_{\text{on}} \\
 & + 0.0140 T_{\text{off}} * T_{\text{off}} - 0.2979 I * I + 0.076 \text{ shape} * \text{shape} - 0.00079 T_{\text{on}} * T_{\text{off}} \\
 & + 0.00781 T_{\text{on}} * I + 0.0035 T_{\text{on}} * \text{shape} + 0.1159 T_{\text{off}} * I - 0.0050 T_{\text{off}} * \text{shape} \\
 & + 0.0103 I * \text{shape}
 \end{aligned} \tag{5}$$

Tables 5 and 6 show the ANOVA and model summary for the CV for Al6061–10% Al<sub>2</sub>O<sub>3</sub>, Al6061–10% SiC, and Al6061–5%Al<sub>2</sub>O<sub>3</sub>–5% SiC respectively. Since the experiments were conducted at 95% confidence level therefore *P* values smaller than 0.05 indicates that the factors has significant effect on the output parameters (Table 5). Similarly, the *P* value of lack of fit should be higher than 0.05 to make it insignificance so that model experimental values fit the

model accurately. The average deviation of the observed values from the regression line is denoted by the standard error of the regression (*S*\*), also known as the standard error of the estimate. As shown in Table 6 lower value of *S*\* and a higher value of *R*-square indicates that model is adequate [49]. Table 5 shows that interaction between *T*<sub>off</sub> and *I* plays a significant role in the CV for all three for all the three composites shown in the experiment.

**Table 5** ANOVA of CV

Source	DF	Al6061–10% Al <sub>2</sub> O <sub>3</sub>			Al6061–10% SiC			Al6061–5% Al <sub>2</sub> O <sub>3</sub> –5% SiC		
		Percentage contribution	F-value	P value	Percentage contribution	F-value	P value	Percentage contribution	F-value	P value
Model	14	92.04	9.91	0.000	92.51	10.59	0.000	96.38	22.83	0.000
Linear	4	55.56	20.94	0.000	56.43	22.61	0.000	59.09	48.98	0.000
T <sub>on</sub>	1	0.19	0.28	0.606	0.14	0.23	0.639	0.00	0.01	0.942
T <sub>off</sub>	1	2.17	3.27	0.096	2.39	3.82	0.074	2.47	8.20	0.014
I	1	53.15	80.12	0.000	53.89	86.36	0.000	56.55	187.50	0.000
Shape	1	0.06	0.08	0.777	0.01	0.01	0.923	0.07	0.23	0.639
Square	4	27.58	10.39	0.001	27.65	11.08	0.001	31.04	25.73	0.000
T <sub>on</sub> *T <sub>on</sub>	1	0.67	0.14	0.719	0.96	0.04	0.847	0.55	0.06	0.808
T <sub>off</sub> *T <sub>off</sub>	1	1.83	0.00	0.956	1.92	0.00	0.979	3.21	0.86	0.372
I*I	1	24.97	34.95	0.000	24.64	36.88	0.000	27.19	76.81	0.000
Shape*shape	1	0.10	0.15	0.709	0.12	0.20	0.664	0.10	0.32	0.585
2-Way interaction	6	8.90	2.24	0.111	8.44	2.25	0.109	6.25	3.45	0.032
T <sub>on</sub> *T <sub>off</sub>	1	0.00	0.01	0.943	0.01	0.01	0.916	0.01	0.02	0.882
T <sub>on</sub> *I	1	0.06	0.09	0.772	0.07	0.12	0.737	0.30	0.99	0.339
T <sub>on</sub> *shape	1	0.00	0.00	0.969	0.00	0.00	0.994	0.01	0.05	0.828
T <sub>off</sub> *I	1	8.55	12.88	<b>0.004</b>	8.09	12.96	<b>0.004</b>	5.92	19.62	<b>0.001</b>
T <sub>off</sub> *shape	1	0.24	0.36	0.561	0.24	0.39	0.546	0.00	0.01	0.925
I*shape	1	0.05	0.08	0.788	0.03	0.04	0.841	0.01	0.02	0.898
Error	12	7.96			7.49			3.62		
Lack-of-fit	10	7.48	3.10	0.269	7.07	3.41	0.248	3.50	5.78	0.157

**3.2 RSM based regression model for SR**

Equations 6, 7, and 8 are the second-order regression model of SR for Al6061–10% Al<sub>2</sub>O<sub>3</sub>, Al 6061–10% SiC, and Al 6061–5% Al<sub>2</sub>O<sub>3</sub>–5% SiC.

$$\begin{aligned}
 \text{SR} = & -1.96 + 0.224 T_{\text{on}} + 0.094 T_{\text{off}} + 1.782 I \\
 & - 0.007 \text{ shape} - 0.00101 T_{\text{on}} * T_{\text{on}} \\
 & + 0.0002 T_{\text{off}} * T_{\text{off}} - 0.1328 I * I \\
 & + 0.345 \text{ shape} * \text{shape} - 0.00421 T_{\text{on}} * T_{\text{off}} \\
 & - 0.00692 T_{\text{on}} * I - 0.0186 T_{\text{on}} * \text{shape} \\
 & - 0.0032 T_{\text{off}} * I + 0.0125 T_{\text{off}} * \text{shape} - 0.2269 I * \text{shape}
 \end{aligned} \tag{6}$$

$$\begin{aligned}
 \text{SR} = & -9.29 + 0.338 T_{\text{on}} + 0.800 T_{\text{off}} + 1.505 I \\
 & + 1.77 \text{ shape} + 0.00012 T_{\text{on}} * T_{\text{on}} \\
 & - 0.0071 T_{\text{off}} * T_{\text{off}} - 0.1664 I * I \\
 & + 0.475 \text{ shape} * \text{shape} - 0.01503 T_{\text{on}} * T_{\text{off}} \\
 & + 0.0003 T_{\text{on}} * I - 0.0675 T_{\text{on}} * \text{shape} \\
 & + 0.0032 T_{\text{off}} * I - 0.0681 T_{\text{off}} * \text{shape} - 0.176 I * \text{shape}
 \end{aligned} \tag{7}$$

**Table 6** Model summary of CV

MMC type	S*	R-sq	R-sq (adj)
Al6061–10% Al <sub>2</sub> O <sub>3</sub>	0.431765	92.04%	82.75%
Al6061–10% SiC	0.427911	92.51%	83.78%
Al6061–5% Al <sub>2</sub> O <sub>3</sub> –5% SiC	0.314006	96.38%	92.16%

$$\begin{aligned}
 \text{SR} = & -5.35 + 0.267 T_{\text{on}} + 0.425 T_{\text{off}} + 1.562 I \\
 & + 0.839 \text{ shape} - 0.00043 T_{\text{on}} * T_{\text{on}} \\
 & - 0.0033 T_{\text{off}} * T_{\text{off}} - 0.1421 I * I \\
 & + 0.389 \text{ shape} * \text{shape} - 0.00914 T_{\text{on}} * T_{\text{off}} \\
 & - 0.00317 T_{\text{on}} * I - 0.0409 T_{\text{on}} * \text{shape} \\
 & + 0.0000 T_{\text{off}} * I - 0.0264 T_{\text{off}} * \text{shape} - 0.1915 I * \text{shape}
 \end{aligned} \tag{8}$$

Tables 7 and 8 show the ANOVA and model summary for the SR of all the three composites. It is observed from Table 7 that P values of lack of fit is greater than 0.05, therefore the regression models given in Eqs. 6, 7, and 8 can accurately



**Table 7** ANOVA of SR

Source	DF	Al6061–10% Al <sub>2</sub> O <sub>3</sub>			Al6061-10%SiC			Al6061–5% Al <sub>2</sub> O <sub>3</sub> –5% SiC		
		Percentage contribution	F-value	P value	Percentage contribution	F-value	P value	Percentage contribution	F-value	P value
Model	14	92.64	10.79	0.000	89.49	7.30	0.001	92.92%	11.25	0.000
Linear	4	52.16	21.27	0.000	47.49	13.55	0.000	50.98%	21.61	0.000
T <sub>on</sub>	1	25.32	41.30	0.000	35.55	40.58	0.000	33.37%	56.59	0.000
T <sub>off</sub>	1	3.23	5.26	0.041	1.57	1.79	0.206	2.35%	3.99	0.069
I	1	23.24	37.90	0.000	8.75	9.99	0.008	15.01%	25.45	0.000
Shape	1	0.38	0.62	0.447	1.62	1.84	0.199	0.25%	0.42	0.527
Square	4	30.01	12.24	0.000	25.89	7.39	0.003	29.37%	12.45	0.000
T <sub>on</sub> *T <sub>on</sub>	1	0.26	0.84	0.377	0.13	0.00	0.951	0.00%	0.13	0.725
T <sub>off</sub> *T <sub>off</sub>	1	0.14	0.00	0.990	0.01	0.12	0.735	0.01%	0.06	0.808
I*I	1	23.63	23.16	0.000	19.88	13.16	0.003	23.00%	22.98	0.000
Shape*shape	1	5.98	9.75	0.009	5.88	6.71	0.024	6.36%	10.78	0.007
2-Way Interaction	6	10.48	2.85	0.058	16.11	3.06	0.047	12.57%	3.55	0.029
T <sub>on</sub> *T <sub>off</sub>	1	0.60	0.98	0.341	3.97	4.53	0.055	2.36%	4.01	0.068
T <sub>on</sub> *I	1	0.72	1.18	0.299	0.00	0.00	0.982	0.13%	0.21	0.652
T <sub>on</sub> *shape	1	1.31	2.14	0.170	8.89	10.15	<b>0.008</b>	5.26%	8.93	<b>0.011</b>
T <sub>off</sub> *I	1	0.01	0.02	0.883	0.01	0.01	0.929	0.00%	0.00	1.000
T <sub>off</sub> *shape	1	0.05	0.09	0.774	0.81	0.93	0.354	0.20%	0.33	0.574
I*shape	1	7.77	12.68	<b>0.004</b>	2.43	2.77	0.122	4.61%	7.82	<b>0.016</b>
Error	12	7.36			10.51			7.08%		
Lack-of-fit	10	6.21	1.08	0.572	7.95	0.62	0.752	5.11%	0.52	0.803

Bold numbers represent the factors having significant effect on the process

**Table 8** Model summary of SR for the fabricated MMCs

MMC Type	S*	R-sq	R-sq(adj)
Al 6061–10% Al <sub>2</sub> O <sub>3</sub>	0.254844	92.64%	84.06%
Al 6061–10% SiC	0.423732	89.49%	77.22%
Al 6061–5% Al <sub>2</sub> O <sub>3</sub> –5% SiC	0.273844	92.92%	84.67%

predict the SR. Similarly higher value of R-sq and R-sq(adj) as depicted in Table 8 indicate the adequacy of developed models. And it is clear that the interaction of I × shape plays a significant role on SR for Al6061–10% Al<sub>2</sub>O<sub>3</sub> and for Al6061–5% Al<sub>2</sub>O<sub>3</sub>–5% SiC combination of T<sub>on</sub> × shape and I × shape plays a significant role and for Al6061–10% SiC combination of T<sub>on</sub> × shape plays a significant role SR.

### 3.3 Parametric analysis of CV

Table 5 shows that interaction between T<sub>off</sub> × I has a significant role in CV irrespective of the type of reinforcements used in the composites. The findings of the RSM plots as shown

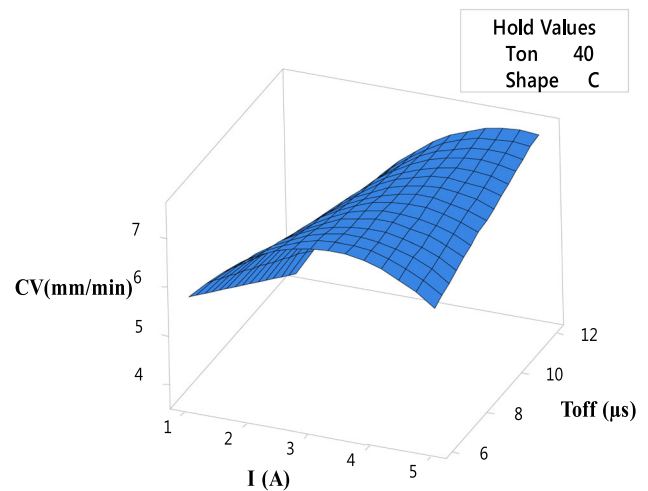


**Fig. 4** RSM plot of CV with respect to T<sub>off</sub> and I for WEDM of Al6061–10% Al<sub>2</sub>O<sub>3</sub>

in Figs. 4, 5, and 6 is given in Table 9. It is observed that increase of current from 1 to 5 A at T<sub>on</sub> = 40 μs and T<sub>off</sub> = 6 μs increases the CV and maximum increase has been noted

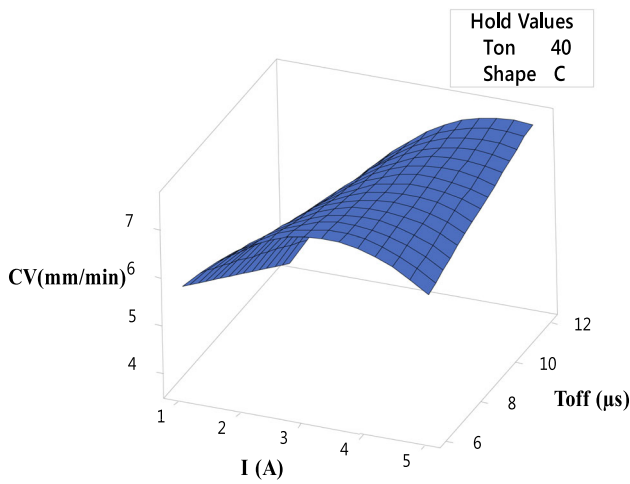


Fig. 5 Surface plot of CV with respect to  $T_{off}$  and  $I$  for WEDM of Al6061–10% SiC

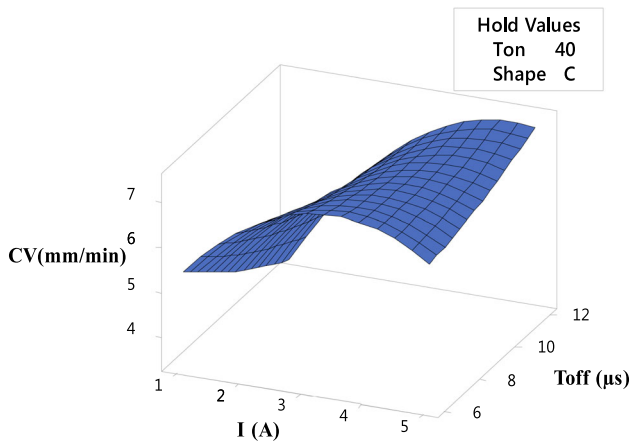


Fig. 6 RSM plot of CV with respect to  $T_{off}$  and  $I$  for WEDM of Al6061–5%  $Al_2O_3$ –5% SiC

Table 9 Effect of input parameters on CV for WEDM of circular profile

Input parameters	Al6061–10% $Al_2O_3$	Al6061–10% SiC	Al6061–5% $Al_2O_3$ –5% SiC
I increase from 1 to 5 A			
$T_{on} = 40 \mu s$ $T_{off} = 6 \mu s$	(+) 9.6%	(+)9.6%	(+)15.2%
$T_{on} = 40 \mu s$ $T_{off} = 12 \mu s$	(+)115%	(+) 115%	(+) 115%
$T_{off}$ increases from 6 $\mu s$ to 12 $\mu s$			
$T_{on} = 40 \mu s$ $I = 1 A$	(–) 48.39%	(–) 48.39%	(–) 45.7%
$T_{on} = 40 \mu s$ $I = 5 A$	No change	No change	No change

for hybrid composite Al6061–5%  $Al_2O_3$ –5% SiC. Similar change of current at higher  $T_{off}$  (12  $\mu s$ ) increases the CV by 115% for all composites irrespective of the type of reinforcements. With the increase of  $T_{off}$  from 6 to 12  $\mu s$  at low current (1 A) reduces the CV in all composites and minimum reduction of 45.7% occurs in hybrid composite whereas at higher current (5 A) the change of  $T_{off}$  has not effect on CV. Therefore a circular profile can be produced at high speed in AMMCs by changing the current at high  $T_{off}$  (12  $\mu s$ ) at constant  $T_{on} = 40 \mu s$ . When the current increases at constant  $T_{on}$  high spark energy is produced which results in increase of melting and material vaporization. The combined effect of high  $T_{on}$  and low  $T_{off}$  lead to more sparking time thus increasing the MRR. But small  $T_{off}$  (6  $\mu s$ ) do not allow the effective flushing of molten material and it also lead to unstable discharge condition; therefore, no significant increase in CV takes place due to rise of current at lower  $T_{off}$ . When  $T_{off}$  increases more stable discharge take place and adequate time is available for flushing of the molten material which lead to significant rise in CV as shown in Table 9. Similarly, increase of  $T_{off}$  at lower current (1A) decreases the CV because at low current spark formation is low and as  $T_{off}$  increases the dielectric fluid begins to deionized and very low material removal take place which finally lead to reduction of CV.

Furthermore for a triangular profile the increase of current from 1 to 5 A at  $T_{on} = 40 \mu s$  and  $T_{off} = 9 \mu s$  increases the CV by 56.5% whereas increase of  $T_{off}$  from 6 to 12  $\mu s$  at  $T_{on} = 40 \mu s$ ,  $I = 3 A$  increases the CV only by 7.24%. Thus for triangular profile, increase of current at constant  $T_{on}$  and  $T_{off}$  has significant effect on CV. For square profile similar variation does not show any major effect on CV [6].

### 3.4 Parametric analysis of SR

Table 7 illustrates that interaction between  $I \times$  shape and  $T_{on} \times$  shape plays a significant role in SR during WEDM of Al6061–10%  $Al_2O_3$  and Al6061–10% SiC respectively. For hybrid composite, both interaction effects play a major role for SR. The summary of the observations given by response plots shown in Figs. 7, 8, 9, and 10 has been depicted in Table 10. It can be observed that during WEDM of different profiles having same perimeter highest SR is produced for triangular profile in all the three composites and minimum SR is obtained for square profile. The results shows that SiC reinforced AMMC produces high SR compared to  $Al_2O_3$  reinforced AMMC. Hybrid composite (Al6061–5%  $Al_2O_3$ –5% SiC) produces low SR for triangular and circular profile compared to other two AMMCs considered in this study whereas in case of square profile an increase in the value of SR has been noted.

The SR increases with the current at constant  $T_{on}$  (40  $\mu s$ ) and  $T_{off}$  (9  $\mu s$ ) because current increases the pulse energy at localized area thereby producing large number of craters

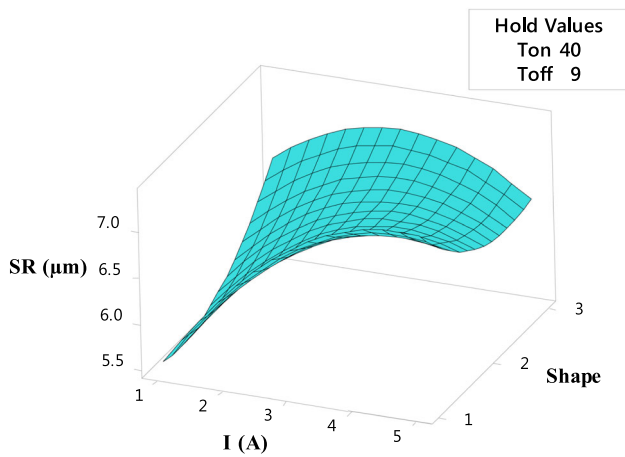


Fig. 7 RSM plots of SR with respect to shape and I for WEDM of Al6061–10% Al<sub>2</sub>O<sub>3</sub>

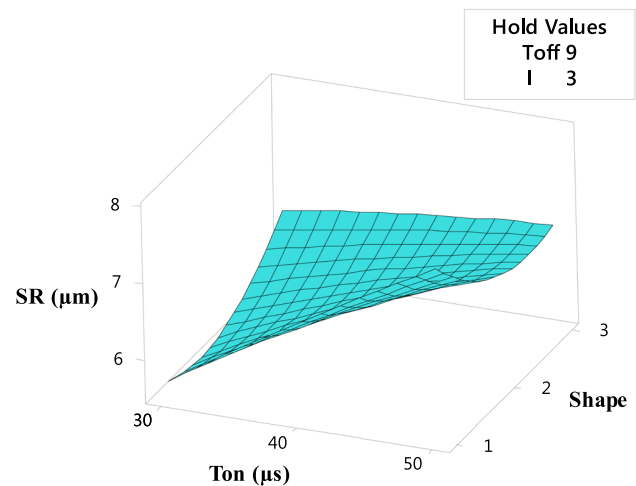


Fig. 10 RSM plot of SR with respect to shape and T<sub>on</sub> for WEDM of Al6061–5% Al<sub>2</sub>O<sub>3</sub>–5% SiC

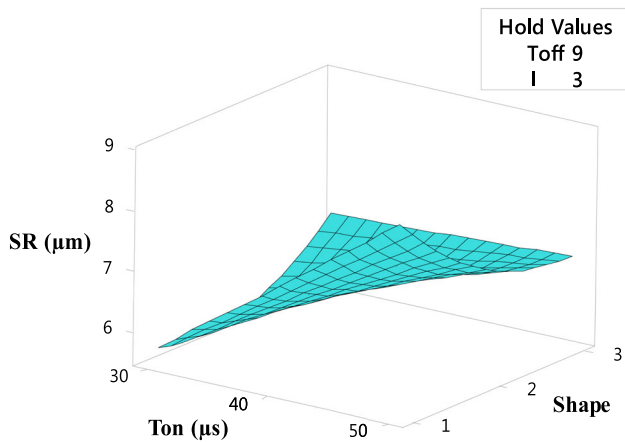


Fig. 8 RSM plots of SR with respect to shape and T<sub>on</sub> for WEDM of Al6061–10% SiC

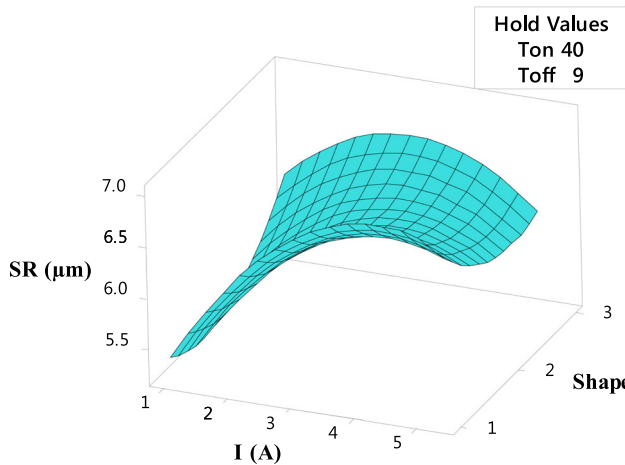


Fig. 9 RSM plot of SR with respect to shape and I for WEDM of Al6061–5% Al<sub>2</sub>O<sub>3</sub>–5% SiC

Table 10 Effect of input parameters on SR for different profiles

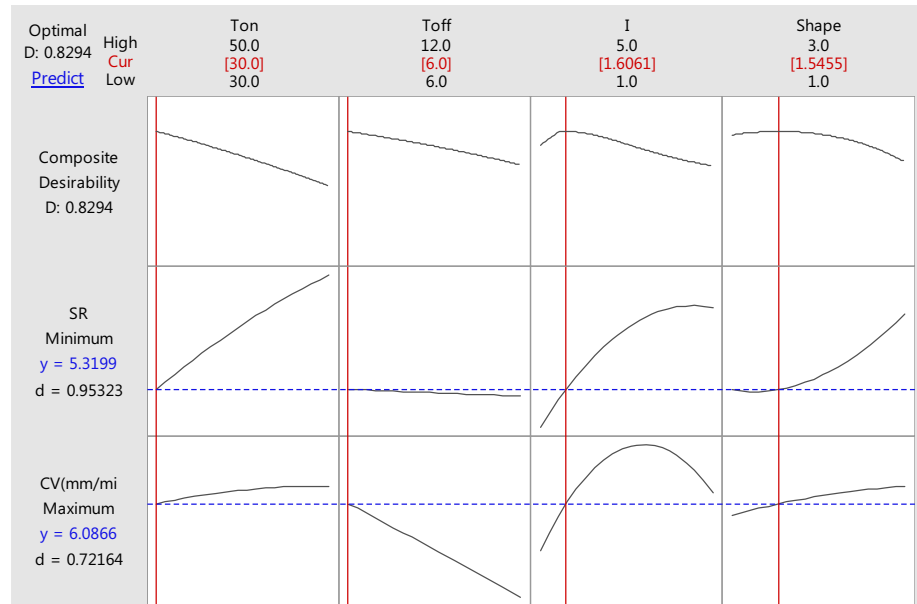
	Circle	Square	Triangle
<i>Al6061–10% Al<sub>2</sub>O<sub>3</sub></i>			
I increase from 1 to 5 A at T <sub>on</sub> = 40 μs and T <sub>off</sub> = 9 μs	14.7%	3.1%	40%
<i>Al6061–10% SiC</i>			
T <sub>on</sub> increases from 30 to 50 μs at T <sub>off</sub> = 9 μs and I = 3 A	26%	3%	53%
<i>Al6061–5% Al<sub>2</sub>O<sub>3</sub>–5% SiC</i>			
I increase from 1 to 5 A at T <sub>on</sub> = 40 μs and T <sub>off</sub> = 9 μs	10.5%	7%	39%
T <sub>on</sub> increases from 30 to 50 μs at T <sub>off</sub> = 9 μs and I = 3 A	20.5%	6.25%	36.4%

on the machined surface. Similarly, when T<sub>on</sub> increases at constant T<sub>off</sub> = 9 μs and I = 3 A, the discharge energy also increases which increases the size of craters on machined surface. In addition to this, the hardness of SiC reinforced particles is high compared to Al<sub>2</sub>O<sub>3</sub>. Both the melting point and thermal conductivity of SiC is quite high compared to Al<sub>2</sub>O<sub>3</sub> therefore, Al6061–10% SiC requires more discharge energy to melt and vaporize the composite. This increases the number of crater produced on the surface and when these craters combined together it increases the SR.

### 3.5 Multi-objective optimization based on RSM modelling

The optimization technique of composite desirability yields a combination of input parameters that provide most desirable output response. Desirability approach of MOO uses an

**Fig. 11** RSM based MOO for Al6061–10% Al<sub>2</sub>O<sub>3</sub>



objective function known as desirability function. This function transform the response into a unitless value ( $d_i$ ) termed as desirability. Here each response is converted into into a desirability function  $d_i$  in the range  $0 \leq d_i \leq 1$ . Higher value of  $d_i$  indicate more desirable response [50]. The desirability value becomes one when the output response achieves its target; otherwise, it becomes zero [51]. The desirability objective function  $D$  is given by Eq. 9.

$$D = (d_1 \times d_2 \times d_3 \dots \dots \dots d_n)^{1/n} \tag{9}$$

$$D = (d^{w1} * d^{w2} * d^{w3} * d^{w4} \dots \dots \dots d^{wn})^{\frac{1}{n}} \tag{10}$$

Each desirability function is assigned a weight whose value changes the polynomial order of the desirability function (Eq. 10). Most statistical software, such as MINITAB, utilizes a reduced gradient algorithm with various starting points to obtain the maximum value of the desirability function [52]. Figures 11, 12, and 13 show the RSM-based MOO for Al6061–10% Al<sub>2</sub>O<sub>3</sub>, Al6061–10% SiC, and Al6061–5% Al<sub>2</sub>O<sub>3</sub>–5% SiC respectively using MINITAB-18. Table 11 shows the MOO input parameters for both material and tool.

### 3.6 Multi objective optimisation based on grey relational analysis

Figure 14 show the flow chart for calculation of GRG value [53]. Table 12 show the calculation of GRC value for the Al6061–10% Al<sub>2</sub>O<sub>3</sub> followed by normalisation of data and deviation sequence. Similarly the value of GRC for other two composites have been evaluated. Table 13 shows the GRG value and their rank based on the higher to lower. Table 14

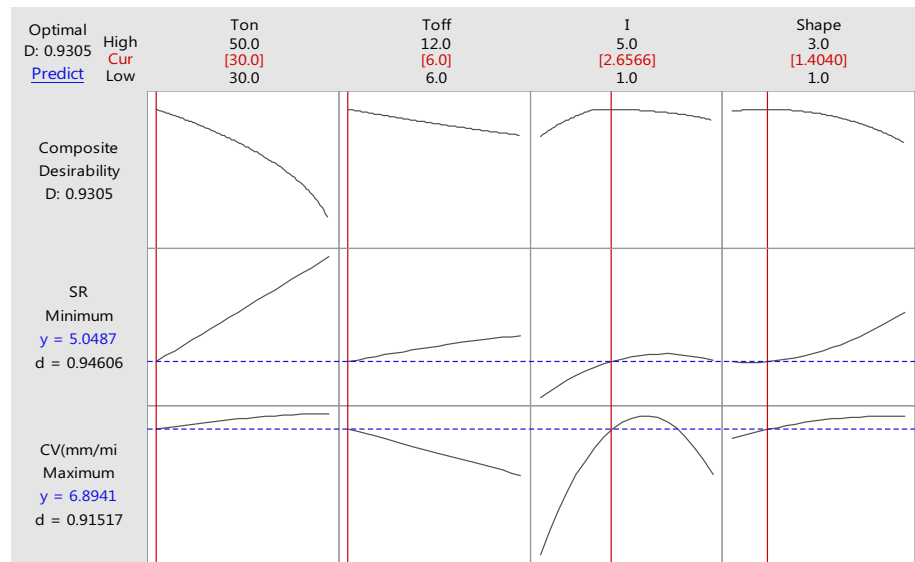
shows the non-optimal input parameters for all the three composites.

### 3.7 Confirmatory experiments

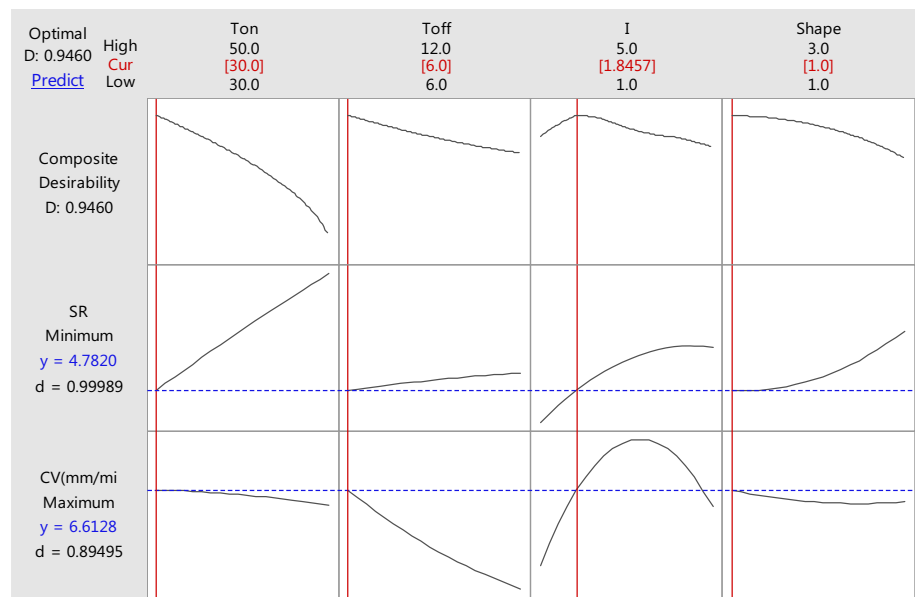
The confirmatory experimental result corresponding to optimal input parameters in Table 11 is shown in Table 15. Table 15 reveals that difference between the predicted optimal values of CV and SR by the composite desirability approach and corresponding confirmatory results obtained after machining of Al6061–10% Al<sub>2</sub>O<sub>3</sub>, Al6061–10% SiC, and Al6061–5% Al<sub>2</sub>O<sub>3</sub>–5% SiC are quite high.

Table 16 shows the comparison between optimal and non-optimal results. The experimental trial yielding highest CV has been chosen as the non-optimized value in Table 15. It is observed that optimal value input parameters occurs only for triangular profile and significant reduction in SR occurs. Addition of Al<sub>2</sub>O<sub>3</sub> and SiC in hybrid AMMC increases the MRR and reduces the SR. The EDS analysis in Fig. 18a shows that silicon content in Al6061–10% Al<sub>2</sub>O<sub>3</sub> reduces by 65% after machining which is responsible for small number of crater formation due to reduction in melting point as shown in Fig. 15b. The SEM image in Fig. 15a also indicates that at non-optimal parameters large number cracks and globules with solidified material whereas at optimal parameters all these formations get reduced due to reduction in oxygen content. Similar observations has been noted during WEDM of Al6061–10% SiC due to reduction of silica and increase of carbon. When carbon increases after machining the thermal conductivity increases due to which heat does not get accumulate and get distribute over a wider range thereby producing small craters responsible for low SR. In case of

**Fig. 12** RSM based MOO for Al6061–10% SiC



**Fig. 13** RSM based MOO for Al6061–5% Al<sub>2</sub>O<sub>3</sub>–5% SiC



**Table 11** Optimal input parameters

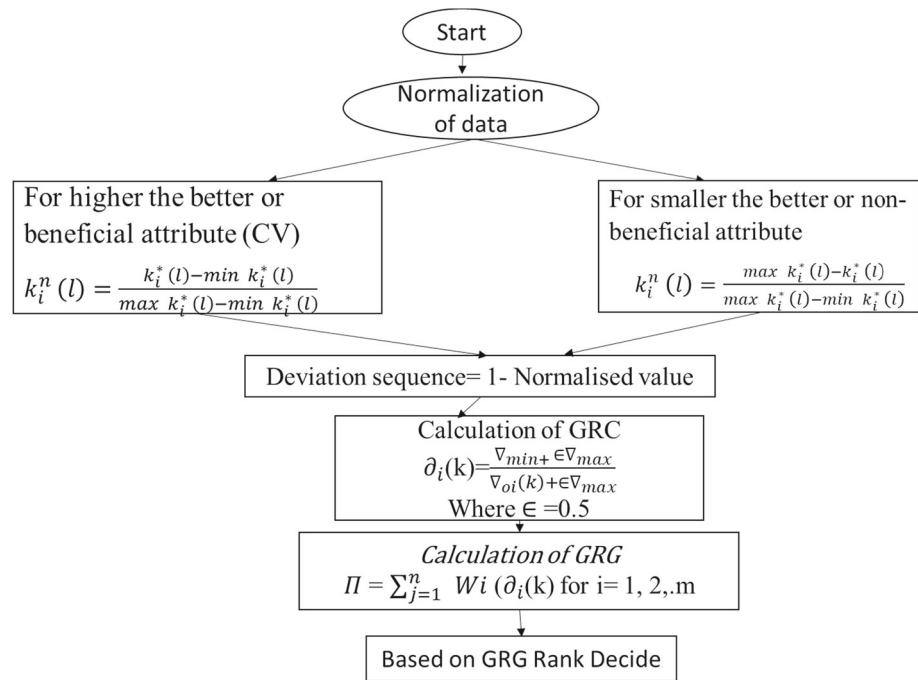
S. no.	Workpiece	T <sub>on</sub>	T <sub>off</sub>	I	Shape	CV	SR
1	Al6061–10% Al <sub>2</sub> O <sub>3</sub>	30	6	1.6061	1.5455	6.0866	5.3199
2	Al6061–10% SiC	30	6	2.6566	1.4040	6.8941	5.0487
3	Al6061–5% Al <sub>2</sub> O <sub>3</sub> –5% SiC	30	6	1.8457	1	6.6128	4.7820

hybrid composites the EDS analysis in Figs. 20 and 21 shows that carbon marginally increases and oxygen content increases significantly with major reduction in silicon content. The combined effect of these parameters can be observed in SEM micrograph in terms reduction in agglomeration of SiC and solidified metal drops.

### 3.8 Morphology of WEDM cut surface

In this section a detail study of the morphological analysis of surface produced by WEDM has been given. Here, surface corresponding to non-optimal input parameters as obtained by GRA has been compared with the surface produced at optimal input parameter as given by RSM-based

Fig. 14 Flow chart for GRG



MOO approach. Scanning electron microscope (JSM 6010 LA, JEOL) has been used for the characterization of WEDM surface. Figures 15, 16, and 17 show the images of surfaces corresponding to WEDM cutting of Al6061–10% Al<sub>2</sub>O<sub>3</sub>, Al6061–10% SiC, and Al6061–5% Al<sub>2</sub>O<sub>3</sub>–5% SiC at non-optimal and optimal input parameters. Figure 15a shows the clear presence of alumina particles on the surface. Larger size solidified metal drops, and larger globules of debris can be seen in the micrographs. This may be due to improper mixing of alumina particles during casting process due to which agglomeration takes place. When the discharge energy and pulse duration increases, more molten material get removed thus producing large craters as shown in Fig. 15 [54]. But at optimal input parameters as shown in Fig. 15b presence of few random micro cracks along with small solidified metal drops has been observed. This results in better surface finish for Al6061–10% Al<sub>2</sub>O<sub>3</sub>. Since at non optimal input parameters T<sub>on</sub> and T<sub>off</sub> are large compared to optimal input parameters, therefore more discharge energy is produced which removes more molten material from the surface thus producing large craters on the surface. Due to higher T<sub>off</sub> there is more time between two successive sparks therefore the molten metal get solidified on the surface thus deteriorating the surface finish. From Table 16 it is found that surface finish at optimal input parameters are 21% lower as compare to non-optimal input parameters.

Similarly, Fig. 16a shows the non-optimal surface of Al6061–10% SiC. SiC is present on the surface and solidified metal drops, globules of debris, gas bubbles, and craters are

present on the surface. Due to this, there are larger irregularities on the surface. Figure 16b shows smaller size solidified metal drops at optimal input parameters. Because at optimal input parameters T<sub>on</sub> and T<sub>off</sub> are lower as compare to non-optimal input parameters, So due to lower T<sub>on</sub> and higher current spark intensity generated for less time so it melt less material on the surface and during T<sub>off</sub> it remove through deionised water, so it give 24.19% better surface finish as compare to non-optimal input parameters.

Figure 17a shows the SEM image of Al6061–5% Al<sub>2</sub>O<sub>3</sub>–5% SiC. Presence of alumina and SiC can be clearly seen on the machined surface. Agglomeration of Alumina and SiC take place and larger size solidified metal drops, and cracks along with gas bubbles are present on the surface. Figure 17b shows the SEM of RSM-based MOO of Al/Al<sub>2</sub>O<sub>3</sub>/SiC, there is alumina and SiC are present on the surface, globules of debris and solidified metal drops are present on the surface, and there are no cracks on the surface are present. Since at non optimal input parameters T<sub>on</sub> is 50 μs and T<sub>off</sub> is 9 μs, so due to spark intensity for larger times it melted the more material on the surface and it remove the excess material from the surface due to this large craters are observed on the surface. And due to larger T<sub>off</sub> value, it produce large size solidified metal drops on the surface as compare to optimal input parameters. From Table 16 it is observed that in case of hybrid MMC it show the better surface finish as compare to all materials and 33.39% better surface quality as compare to non-optimal input parameters.

**Table 12** Calculation of GRC for Al6061-10% Al<sub>2</sub>O<sub>3</sub>

S. no.	Normalized value		Devition sequence		GRC	
	CV	SR	CV	SR	CV	SR
1	0.885106	0.682979	0.114894	0.317021	0.813149	0.611979
2	0.929258	0.137589	0.070742	0.862411	0.876052	0.366996
3	0.863866	0.62766	0.136134	0.37234	0.785997	0.573171
4	0.892308	0.297163	0.107692	0.702837	0.822785	0.415684
5	0.3	0.943972	0.7	0.056028	0.416667	0.899235
6	0.921739	0.053901	0.078261	0.946099	0.864662	0.345758
7	0.344509	0.506383	0.655491	0.493617	0.432716	0.503212
8	0.906897	0.388652	0.093103	0.611348	0.843023	0.449904
9	0.870886	0.652482	0.129114	0.347518	0.794769	0.589958
10	0.921739	0.089362	0.078261	0.910638	0.864662	0.354449
11	0.85	0.263121	0.15	0.736879	0.769231	0.404243
12	0.892308	0.017021	0.107692	0.982979	0.822785	0.337159
13	0.752941	0.699291	0.247059	0.300709	0.669291	0.624446
14	0	0.832624	1	0.167376	0.333333	0.749203
15	0.892308	0.319858	0.107692	0.680142	0.822785	0.423678
16	0.914286	0.485816	0.085714	0.514184	0.853659	0.493007
17	0.389189	1	0.610811	0	0.450122	1
18	0.4375	0.51773	0.5625	0.48227	0.470588	0.509025
19	0.975785	0.592908	0.024215	0.407092	0.953807	0.551212
20	0.96	0.346099	0.04	0.653901	0.925926	0.433313
21	0.870886	0	0.129114	1	0.794769	0.333333
22	0.991855	0.260993	0.008145	0.739007	0.983972	0.403549
23	1	0.166667	0	0.833333	1	0.375
24	0.991855	0.36383	0.008145	0.63617	0.983972	0.440075
25	0.983784	0.475177	0.016216	0.524823	0.968586	0.487889
26	0.967857	0.356738	0.032143	0.643262	0.939597	0.437345
27	0.863866	0.265957	0.136134	0.734043	0.785997	0.405172

### 3.9 Energy dispersive spectroscopy (EDS)

In this study, the chemical composition of all workpiece before and after machining has been performed by EDS analysis using SEM (JSM 6010 LA, JEOL). Figures 18 and 19 respectively shows the EDS graph and chemical composition Al6061–10% Al<sub>2</sub>O<sub>3</sub> before and after machining. It is observed that oxygen content increases from 19.90 to 27.72% after machining thus indicating oxidation phenomena at the cut surface. It is observed that due to machining the Al contents decreases by 8% whereas largest reduction of approx. 65% occurs for Si-content.

Similarly, Figs. 20a, b and 21a, b depicts that after machining AMMC/SiC surface shows that carbon content get enhanced by 14% whereas reduction in Al and Si has been observed. EDS results of Al6061–10% Al<sub>2</sub>O<sub>3</sub> shows the presence of oxygen and Aluminum whereas for Al6061–10% SiC the composite mainly contains carbon and aluminum.

Figures 22 and 23 show the elemental composition of fabricated hybrid composites i.e., Al6061–5% Al<sub>2</sub>O<sub>3</sub>–5%SiC. It elucidates that the composite mainly contains carbon, oxygen and aluminium. WEDM of this composite primarily increases the oxygen content and major drop in Aluminium content take place. Unlike Al6061–10% SiC the carbon content does not show any appreciable change due to machining of Al6061–5% Al<sub>2</sub>O<sub>3</sub>–5%SiC.

### 4 Conclusions

In this study, a comparative analysis for the WEDM of AMMCs with different compositions have been performed. Three different AMMCs i.e. Al6061–10% Al<sub>2</sub>O<sub>3</sub>, Al6061–10% SiC and Al6061–5% Al<sub>2</sub>O<sub>3</sub>–5%SiC were fabricated by stir casting method. Three different geometrical

**Table 13** GRG and rank

S. no.	Al6061–10% Al <sub>2</sub> O <sub>3</sub>		Al6061–10% SiC		Al6061–5%Al <sub>2</sub> O <sub>3</sub> –5% SiC	
	GRG	Rank	GRG	Rank	GRG	Rank
1	0.712564	4	0.766155	5	0.786121	2
2	0.621524	17	0.617113	21	0.673358	16
3	0.679584	11	0.690046	13	0.715522	8
4	0.619234	18	0.644039	18	0.665065	19
5	0.657951	13	0.56378	25	0.595253	24
6	0.60521	20	0.652715	16	0.666508	18
7	<b>0.467964</b>	<b>27</b>	<b>0.483749</b>	<b>27</b>	0.46591	26
8	0.646464	15	0.648622	17	0.694865	12
9	0.692363	7	0.776099	2	0.788301	1
10	0.609556	19	0.610065	23	0.650872	20
11	0.586737	22	0.639734	19	0.640821	22
12	0.579972	23	0.65689	15	0.668929	17
13	0.646869	14	0.681705	14	0.645599	21
14	0.541268	25	0.587139	24	0.564711	25
15	0.623231	16	0.718703	10	0.703991	10
16	0.673333	12	0.774735	3	0.764558	4
17	0.725061	3	0.725389	9	0.715754	7
18	0.489807	26	0.517577	26	<b>0.456567</b>	<b>27</b>
19	0.752509	1	0.866901	1	0.779997	3
20	0.679619	10	0.69972	11	0.68681	14
21	0.564051	24	0.626125	20	0.688742	13
22	0.69376	6	0.698717	12	0.684627	15
23	0.6875	9	0.736702	8	0.709919	9
24	0.712023	5	0.755057	6	0.720435	6
25	0.728238	2	0.772779	4	0.727295	5
26	0.688471	8	0.742223	7	0.699931	11
27	0.595585	21	0.616469	22	0.619156	23

Bold values represent the experimental run with lowest GRG value thus indicating the combination of input process parameters which yield the worst output characteristics

**Table 14** Non optimal input parameters

S. no.	Composites	T <sub>on</sub>	T <sub>off</sub>	I	Shape
1	Al6061–10% Al <sub>2</sub> O <sub>3</sub>	40	9	1	S
2	Al6061–10% SiC	40	9	1	S
3	Al6061–5% Al <sub>2</sub> O <sub>3</sub> –5% SiC	50	9	1	C

profiles having same perimeter were produced in these composites using WEDM. In order to analyse the effect of input process parameters during WEDM of different profiles in AMMCs having different composition BBD based RSM models were developed and optimal inputs parameters were determined using the desirability approach of RSM. The change in surface characteristics and elemental composition due to WEDM of these composites have been carried out using SEM. BBD based second order regression model to

establish the relation between the input parameters (T<sub>on</sub>, T<sub>off</sub>, I and shape) and output parameters (SR and CV) have been developed and following conclusions can be drawn based on this study:

- a. The experimental findings reveals that interaction between T<sub>off</sub> × I plays a significant role in CV irrespective of the composition of AMMCs. Increase of T<sub>off</sub> from 6 to 12 μs at T<sub>on</sub> = 40 μs and I = 1 A reduces

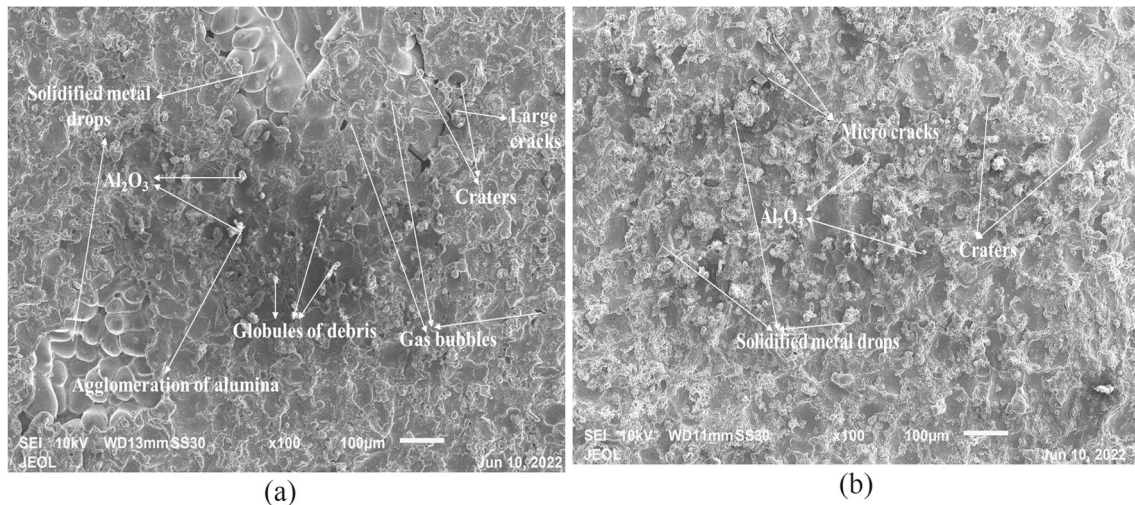


**Table 15** Confirmatory experiment for composite desirability optimal results

S. no.	Workpiece material	$T_{on}$	$T_{off}$	I	Shape	Predicted optimal result		Confirmatory result		% Change in CV	% Change in SR
						CV	SR	CV	SR		
1	Al6061–10% Al <sub>2</sub> O <sub>3</sub>	30	6	2	T	6.0866	5.3199	7.0714	5.6448	16.18	6.11
2	Al6061–10% SiC	30	6	3	T	6.8941	5.0487	7.135	5.1824	3.49	2.64
3	Al6061–5% Al <sub>2</sub> O <sub>3</sub> –5% SiC	30	6	2	T	6.6128	4.7820	7.04	4.884	6.46	2.13

**Table 16** Comparison of optimal and non-optimal results

S. no.	Workpiece material	Non-optimized value			Optimized value			% Change in CV	% Change in SR
		Shape	CV	SR	Shape	CV	SR		
1	Al6061–10% Al <sub>2</sub> O <sub>3</sub>	S	7.2	7.1683	T	7.0714	5.6448	(–) 1.8	(–) 21
2	Al6061–10% SiC	S	7.2328	6.8366	T	7.135	5.1824	(–) 1.3	(–) 24.19
3	Al6061–5% Al <sub>2</sub> O <sub>3</sub> –5% SiC	C	7.0	7.3324	T	7.04	4.884	(+) 0.57	(–) 33.39

**Fig. 15** SEM of Al6061–10% Al<sub>2</sub>O<sub>3</sub>: **a** at non-optimal parameters ( $T_{on}$ : 40  $\mu$ s,  $T_{off}$ : 9  $\mu$ s, I: 1 A) for square shape and **b** at optimal input parameter ( $T_{on}$ : 30  $\mu$ s,  $T_{off}$ : 6  $\mu$ s, I: 2 A) for triangular shape

- CV by 48.39% in Al6061–10% Al<sub>2</sub>O<sub>3</sub> and Al6061–10% SiC respectively. The corresponding decrease in hybrid composite Al6061–5% Al<sub>2</sub>O<sub>3</sub>–5% SiC is 45.7%. But at higher current (5 A), CV is not affected by change of  $T_{off}$  for all three composites.
- b. When current increases from 1 to 5 A at  $T_{on} = 40 \mu$ s and  $T_{off} = 12 \mu$ s, the CV shows appreciable increase of 115% in all the three composites whereas similar change

- at lower  $T_{off}$  (6  $\mu$ s) enhances this CV by 9.6% only in Al6061–10% Al<sub>2</sub>O<sub>3</sub> and Al6061–10% SiC.
- c. SR of all three composites increases by increasing either current or  $T_{on}$ . When current increases from 1 to 5 A (at  $T_{on} = 40 \mu$ s and  $T_{off} = 9 \mu$ s) the SR of triangular profile increases by 40% in Al6061–10% Al<sub>2</sub>O<sub>3</sub>. When  $T_{on}$  increases from 30 to 50  $\mu$ s at  $T_{off} = 9 \mu$ s and I = 3 A the SR of triangular profile in Al6061–10% SiC

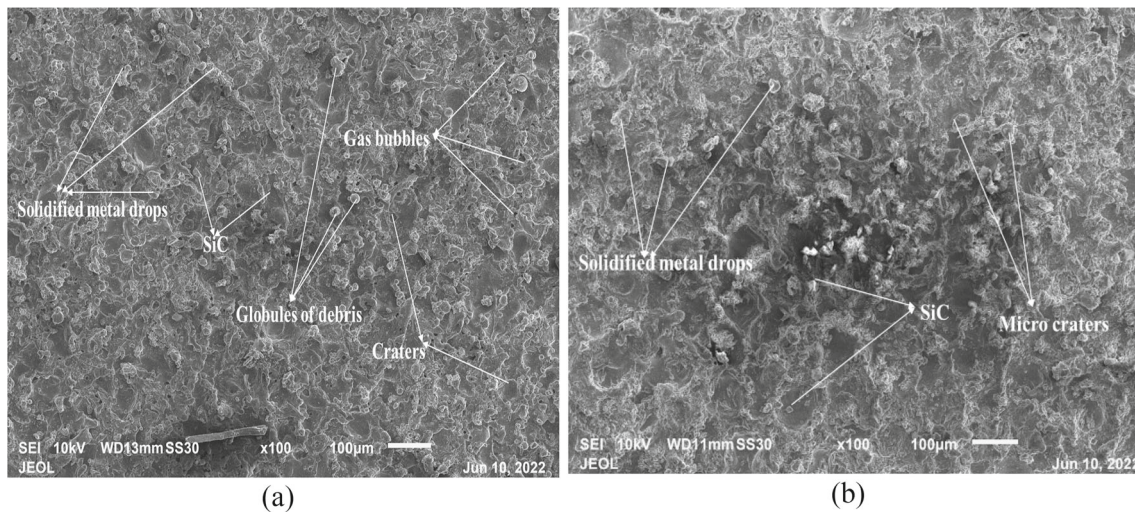


**Fig. 16** SEM of Al6061–10% SiC **a** at non optimal parameters ( $T_{on}$ : 40  $\mu$ s,  $T_{off}$ : 9  $\mu$ s, I: 1 A) for square shape and **b** at optimal input parameters ( $T_{on}$ : 30  $\mu$ s,  $T_{off}$ : 6  $\mu$ s, I: 3 A) for triangular shape

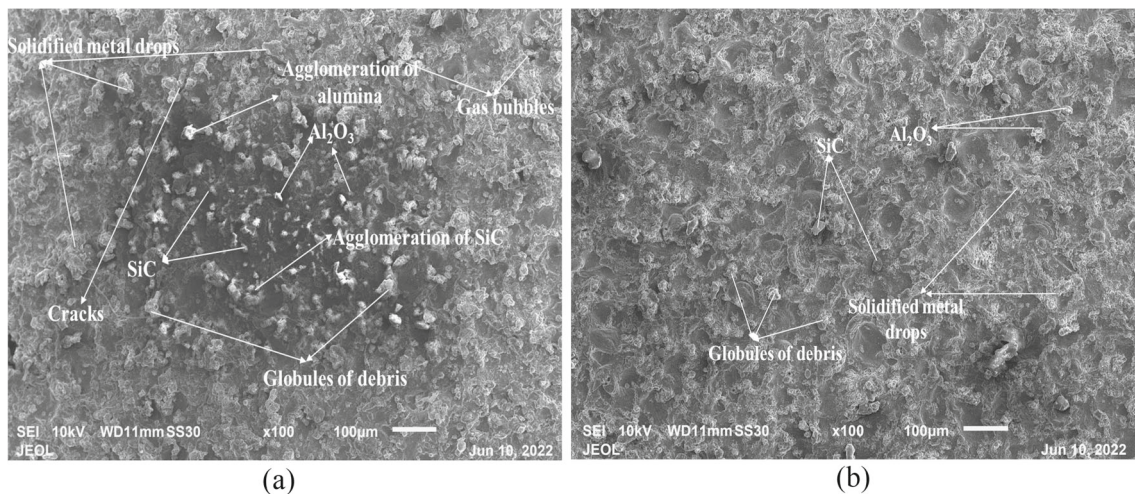
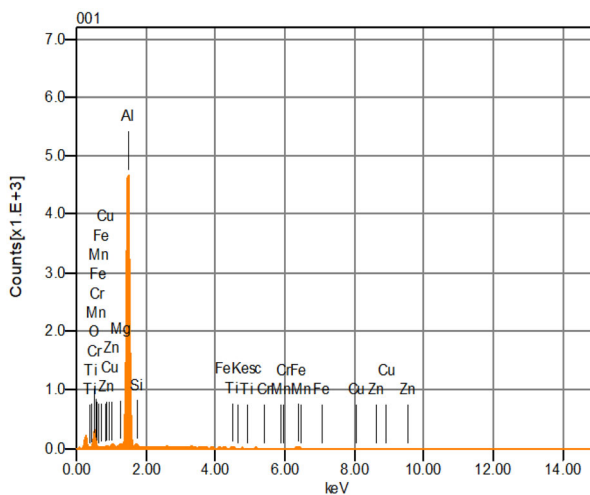


**Fig. 17** SEM of hybrid Al6061–5%  $Al_2O_3$ –5% SiC **a** at non-optimal input parameters ( $T_{on}$ : 50  $\mu$ s,  $T_{off}$ : 9  $\mu$ s, I: 1 A) for circle shape **b** at non-optimal input parameters ( $T_{on}$ : 30  $\mu$ s,  $T_{off}$ : 6  $\mu$ s, I: 2 A) for triangular shape

- increases by 53%. The similar change in hybrid composite Al6061–5%  $Al_2O_3$ –5% SiC increases the SR of triangular profile by 39% and 36.4% respectively.
- d. MOO using composite desirability approach of RSM shows that in contrast to individual addition of alumina and silica, addition of 5 wt% of both reinforcement in AMMC reduces the SR of machining without any significant reduction in its CV.
  - e. EDS analysis shows that after WEDM of Al6061–10%  $Al_2O_3$  the oxygen content increases from 19.99 to 27.72% whereas the mass percentage composition of aluminium and silicon reduces. WEDM of Al6061–10% SiC shows enhancement of carbon and reduction of aluminium and Silica. In case hybrid composite both carbon

- and oxygen content increases after machining while the aluminium shows highest relative reduction.
- f. SEM micrograph of surface corresponding to optimal input parameters shows few micro cracks along with small, solidified metal drops has been observed for all the three composites.

**Fig. 18** a EDS and b chemical composition Al6061–10% Al<sub>2</sub>O<sub>3</sub> before machining

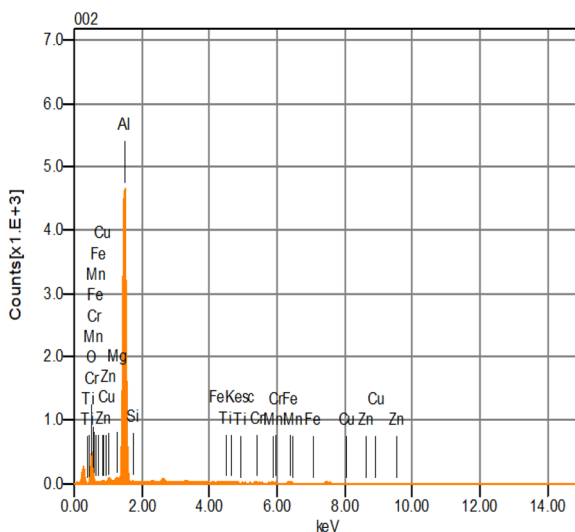


(a)

Elements	Mass %	Atom %
O	19.90	29.89
Mg	0.30	0.29
Al	74.61	66.45
Si	2.66	2.27
Ti	0.30	0.15
Cr	0.33	0.15
Mn	0.05	0.02
Fe	1.27	0.55
Zn	0.59	0.22
Total	100	100

(b)

**Fig. 19** a EDS and b chemical composition of Al6061–10% Al<sub>2</sub>O<sub>3</sub> after machining triangular profile at (T<sub>on</sub>: 30 μs, T<sub>off</sub>: 6 μs, I: 2 A)



(a)

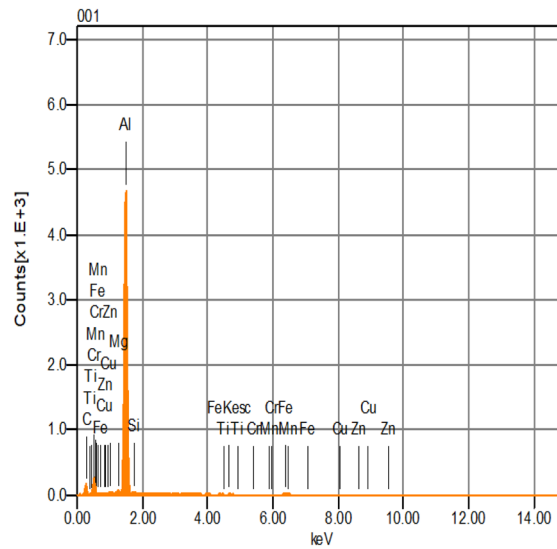
Elements	Mass %	Atom %
O	27.72	39.54
Mg	0.81	0.76
Al	68.88	58.27
Si	0.92	0.75
Ti	0.08	0.04
Cr	0.11	0.05
Mn	0.24	0.10
Fe	1.07	0.44
Cu	0.07	0.03
Zn	0.12	0.04
Total	100	100

(b)

It is suggested from the above study that in order to create different profiles of same perimeter in AMMCs of various composition the current should be increased at constant T<sub>on</sub> (40 μs) and T<sub>off</sub> (12 μs). The study also suggests that SR

of machined surface changes significantly for different geometrical profiles and at the similar input conditions, a square profile produces lowest SR whereas a triangular profiles produce highest SR.

**Fig. 20** a EDS and b chemical composition Al6061–10% SiC before machining

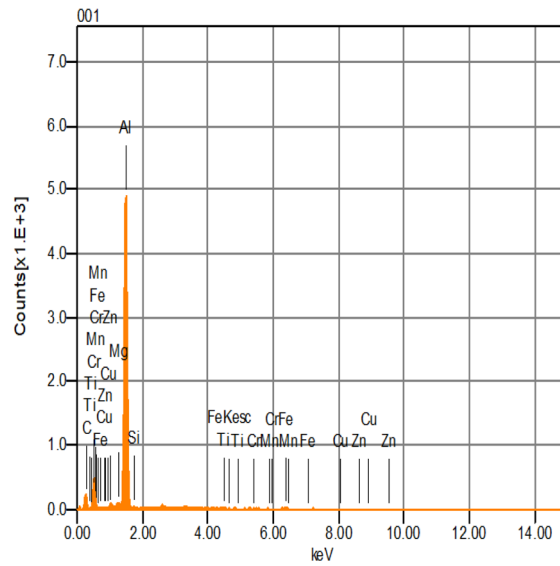


(a)

Elements	Mass %	Atom %
C	46.16	66.16
Mg	0.18	0.13
Al	50.97	32.52
Si	1.22	0.75
Cr	0.03	0.01
Mn	0.12	0.04
Fe	1.21	0.37
Zn	0.10	0.03
Total	100	100

(b)

**Fig. 21** a EDS and b chemical composition of Al6061–10% SiC after machining triangular profile at ( $T_{on} = 30 \mu s$ ,  $T_{off} = 6 \mu s$ ,  $I = 3 A$ )

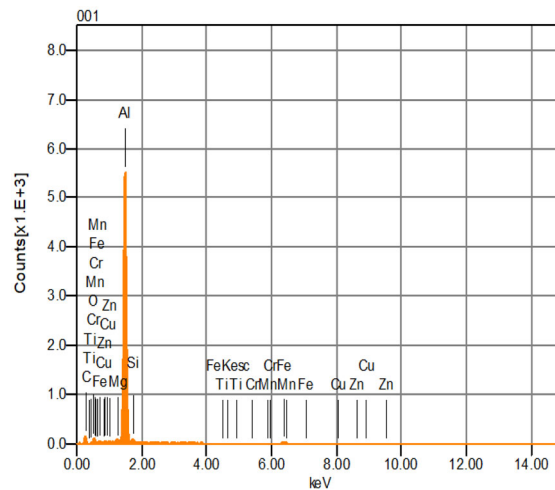


(a)

Elements	Mass %	Atom %
C	52.44	71.47
Mg	0.57	0.38
Al	45.31	27.48
Si	0.62	0.36
Ti	0.14	0.05
Mn	0.11	0.03
Fe	0.49	0.14
Cu	0.16	0.04
Zn	0.17	0.04
Total	100	100

(b)

**Fig. 22** a EDS and b chemical composition Al6061–5% Al<sub>2</sub>O<sub>3</sub>–5%SiC before machining

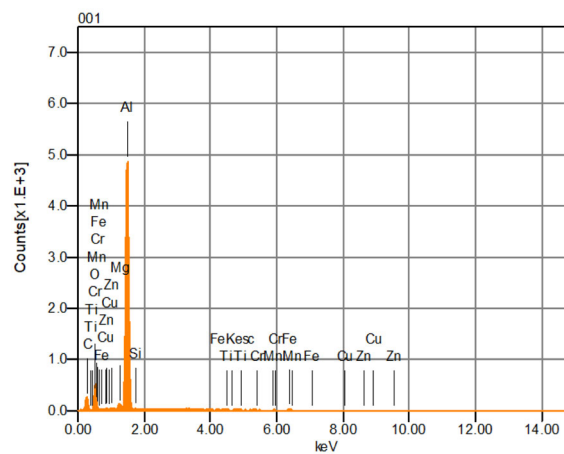


(a)

Elements	Mass %	Atom %
C	36.75	54.97
O	7.86	8.83
Mg	0.38	0.28
Al	51.39	34.22
Si	1.71	1.09
Ti	0.05	0.02
Mn	0.15	0.05
Fe	1.51	0.48
Cu	0.07	0.02
Zn	0.14	0.04
Total	100	100

(b)

**Fig. 23** a EDS and b chemical composition of Al6061–5% Al<sub>2</sub>O<sub>3</sub>–5%SiC after machining triangular profile at (T<sub>on</sub> = 30 μs, T<sub>off</sub> = 6 μs, I = 2 A)



(a)

Elements	Mass %	Atom %
C	37.40	51.56
O	24.14	24.98
Mg	0.70	0.48
Al	36.66	22.50
Si	0.53	0.31
Ti	0.11	0.04
Cr	0.06	0.02
Mn	0.01	0.00
Fe	0.24	0.07
Zn	0.14	0.04
Total	100	100

(b)

**Acknowledgements** The All India Council for Technical Education's (AICTE) 2019-20 Research Promotion Scheme (File No. 8-104/FDC/RPS(POLICY-1)/2019-20) funding help is gratefully acknowledged by the authors.

**Author contributions** DPS: conceived of the presented idea. He conducted the experiments and performed the computations. DPS: wrote the manuscript with the support of SM. SM: supervised the findings of this work. All authors discussed the results and contributed to the final manuscript.

**Availability of data and material** Not applicable.

**Code availability** Not applicable.

## Declarations

**Conflict of interest** The authors have no conflicts of interest to declare. All co-authors have seen and agree with the contents of the manuscript and there are no financial or non-financial interest. Directly related to the submitted work. Both the authors hereby certify that the submission is original work and is not under review at any other publication.

## References

1. Surappa, M.K.: Aluminium matrix composites: challenges and opportunities. *Sadhana* **28**(1), 319–334 (2003). <https://doi.org/10.1007/BF02717141>
2. Zolotova, D., Serpova, V., Prokofiev, M., Rabinskiy, L., Shavnev, A.: A study of the composition and microstructure of aluminum matrix composites reinforced with alumina fibers. *IOP Conf. Ser. Mater. Sci. Eng.* **124**(1), 012135 (2016). <https://doi.org/10.1088/1757-899X/124/1/012135>
3. Miracle, D.B.: Metal matrix composites—from science to technological significance. *Compos. Sci. Technol.* **65**(15–16), 2526–2540 (2005). <https://doi.org/10.1016/j.compscitech.2005.05.027>
4. Ahmad, Z.: Mechanical behavior and fabrication characteristics of aluminum metal matrix composite alloys. *J. Reinf. Plast. Compos.* **20**(11), 921–944 (2001). <https://doi.org/10.1177/073168401772678896>
5. Teng, X., Huo, D.: Conventional machining of metal matrix composites. In: *Advances in machining of composite materials: conventional and non-conventional processes*, pp. 159–181. Springer, Cham (2021)
6. Darji, Y., Patel, D., Patel, D., Ramesh, R., Oza, A.D., Bhole, K.S., Shinde, S.M., Kumar, M.: Experimentation with the EDM parameter through a full factorial technique and optimization using

- regression analysis with carbon nanotubes. *Int. J. Interact. Des. Manuf. (IJIDeM)* (2023). <https://doi.org/10.1007/s12008-023-01263-2>
7. Goyal, K.K., Sharma, N., Dev Gupta, R., Singh, G., Rani, D., Banga, H.K., Giasin, K.: A soft computing-based analysis of cutting rate and recast layer thickness for AZ31 alloy on WEDM using RSM-MOPSO. *Materials* **15**(2), 635 (2022). <https://doi.org/10.3390/ma15020635>
  8. Bagal, D.K., Barua, A., Jeet, S., Satapathy, P., Patnaik, D.: MCDM optimization of parameters for wire-EDM machined stainless steel using hybrid RSM-TOPSIS, genetic algorithm and simulated annealing. *Int. J. Eng. Adv. Technol.* **9**(1), 366–371 (2019). <https://doi.org/10.35940/ijeat.A9349.109119>
  9. Naidu, B.V.V., Varaprasad, K.C., Rao, K.P.: Development of regression models for wire electrical discharge machining of aluminium metal matrix composites. *Mater. Today Proc.* **39**(1), 236–239 (2021). <https://doi.org/10.1016/j.matpr.2020.06.586>
  10. Abhilash, P.M., Chakradhar, D.: Multi-response optimization of wire EDM of Inconel 718 using a hybrid entropy weighted GRA-TOPSIS method. *Process Integr. Optim. Sustain.* **6**(1), 61–72 (2022). <https://doi.org/10.1007/s41660-021-00202-6>
  11. Magesh, M., Jyothiraj, K., Janarthanan, G., Keerthivasan, C., Sivaraman, P.: Optimization of wire-EDM parameters to calculate MRR and measure surface finish on SS410. *Int. J. Innov. Sci. Res. Technol.* **2**(3), 2456–2165 (2017)
  12. Sadhasivam, R.M., Ramanathan, K.: Investigating the parametric effects and analysis of stir cast aluminium matrix composite by Wirecut-EDM using Topsis method. *Sadhana* **46**(3), 1–10 (2021). <https://doi.org/10.1007/s12046-021-01674-5>
  13. Kumar, A., Grover, N., Manna, A., Chohan, J.S., Kumar, R., Singh, S., Pruncu, C.I.: Investigating the influence of WEDM process parameters in machining of hybrid aluminum composites. *Adv. Compos. Lett.* (2020). <https://doi.org/10.1177/2633366X20963137>
  14. Paul, R.C., Joseph, R., Nadana Kumar, V., Booma Devi, P., Manigandan, S.: Experimental analysis of hybrid metal matrix composite reinforced with Al<sub>2</sub>O<sub>3</sub> and graphite. *Int. J. Amb. Energy* **43**(1), 648–652 (2022). <https://doi.org/10.1080/01430750.2019.1653984>
  15. Sivananthan, S., Ravi, K., Samuel, C.S.: Effect of SiC particles reinforcement on mechanical properties of aluminium 6061 alloy processed using stir casting route. *Mater. Today Proc.* **21**, 968–970 (2020). <https://doi.org/10.1016/j.matpr.2019.09.068>
  16. Sivananthan, S., Reddy, V.R., Samuel, C.S.: Preparation and evaluation of mechanical properties of 6061Al-Al<sub>2</sub>O<sub>3</sub> metal matrix composites by stir casting process. *Mater. Today Proc.* **21**, 713–716 (2020). <https://doi.org/10.1016/j.matpr.2019.06.744>
  17. Kumar, A., Grover, N., Manna, A., Kumar, R., Chohan, J.S., Singh, S., Pruncu, C.I.: Multi-objective optimization of WEDM of aluminium hybrid composites using AHP and genetic algorithm. *Arab. J. Sci. Eng.* **47**(7), 8031–8043 (2022). <https://doi.org/10.1007/s13369-021-05865-4>
  18. Lal, S., Kumar, S., Khan, Z.A., Siddiquee, A.N.: Multi-response optimization of wire electrical discharge machining process parameters for Al7075/Al<sub>2</sub>O<sub>3</sub>/SiC hybrid composite using Taguchi-based grey relational analysis. *Proc. Inst. Mech. Eng. Part B J. Eng. Manuf.* **229**(2), 229–237 (2015). <https://doi.org/10.1177/0954405414526382>
  19. Raju, K., Balakrishnan, M., Priya, C.B., Sivachitra, M., Narasimha Rao, D.: Parametric optimization of wire electrical discharge machining in AA7075 metal matrix composite. *Adv. Mater. Sci. Eng.* (2022). <https://doi.org/10.1155/2022/4438419>
  20. Tapadar, J., Thakur, R., Chetia, P., Tamang, S.K., Samanta, S.: Modeling of WEDM parameters while machining Mg-SiC metal matrix composite. *Mech. Eng.* (2017). <https://doi.org/10.14716/ijtech.v8i5.870>
  21. Singh, H., Garg, R.: Effects of process parameters on material removal rate in WEDM. *J. Achiev. Mater. Manuf. Eng.* **32**(1), 70–74 (2009)
  22. Khanna, R., Sharma, N., Kumar, N., Gupta, R.D., Sharma, A.: WEDM of Al/SiC/Ti composite: a hybrid approach of RSM-ARAS-TLBO algorithm. *Int. J. Lightw. Mater. Manuf.* **5**(3), 315–325 (2022). <https://doi.org/10.1016/j.ijlmm.2022.04.003>
  23. Beck, R.J., Aspinwall, D.K., Soo, S.L., Williams, P., Perez, R.: Fatigue performance of surface ground and wire electrical discharge machined TiNi shape memory alloy. *Proc. Inst. Mech. Eng. Part B J. Eng. Manuf.* **236**(4), 355–362 (2022). <https://doi.org/10.1177/09544054211028844>
  24. Pramanik, A., Islam, M.N., Boswell, B., Basak, A.K., Dong, Y., Littlefair, G.: Accuracy and finish during wire electric discharge machining of metal matrix composites for different reinforcement size and machining conditions. *Proc. Inst. Mech. Eng. Part B J. Eng. Manuf.* **232**(6), 1068–1078 (2018). <https://doi.org/10.1177/0954405416662079>
  25. Straka, L., Corny, I.: Adjustment of wire vibrations in order to improve geometric accuracy and surface roughness at WEDM. *Appl. Sci.* **11**(11), 4734 (2021). <https://doi.org/10.3390/app1114734>
  26. Sadeghi, M., Razavi, H., Esmaeilzadeh, A., Kolahan, F.: Optimization of cutting conditions in WEDM process using regression modelling and Tabu-search algorithm. *Proc. Inst. Mech. Eng. Part B J. Eng. Manuf.* **225**(10), 1825–1834 (2011). <https://doi.org/10.1177/0954405411406639>
  27. Singh, D.P., Mishra, S., Yadav, S.K.S., Porwal, R.K., Singh, V.: Comparative analysis and optimization of thermoelectric machining of alumina and silicon carbide-reinforced aluminum metal matrix composites using different electrodes. *J. Adv. Manuf. Syst.* (2022). <https://doi.org/10.1142/S0219686723500191>
  28. Joy, R., Manoj, I.V., Narendranath, S.: Investigation of cutting speed, recast layer and micro-hardness in angular machining using slant type taper fixture by WEDM of Hastelloy X. *Mater. Today Proc.* **27**, 1943–1946 (2020). <https://doi.org/10.1016/j.matpr.2019.09.021>
  29. Nayak, B.B., Mahapatra, S.S.: A utility concept approach for multi-objective optimization of taper cutting operation using WEDM. *Procedia Eng.* **97**, 469–478 (2014). <https://doi.org/10.1016/j.proeng.2014.12.271>
  30. Manoj, I.V., Narendranath, S.: Effect of profile geometry and cutting speed override parameter on profiling speed during tapering using wire electric discharge machining. In: Sustainable machining strategies for better performance, pp. 111–122. Springer (2022)
  31. Manoj, I.V., Soni, H., Narendranath, S., Mashinini, P.M., Kara, F.: Examination of machining parameters and prediction of cutting velocity and surface roughness using RSM and ANN using WEDM of Altemp HX. *Adv. Mater. Sci. Eng.* (2022). <https://doi.org/10.1155/2022/5192981>
  32. Selvakumar, G., BravilinJiju, K., Sarkar, S., Mitra, S.: Enhancing die corner accuracy through trim cut in WEDM. *Int. J. Adv. Manuf. Technol.* **83**(5), 791–803 (2016). <https://doi.org/10.1007/s00170-015-7606-0>
  33. Devarajaiah, D., Muthumari, C.: Evaluation of power consumption and MRR in WEDM of Ti–6Al–4V alloy and its simultaneous optimization for sustainable production. *J. Braz. Soc. Mech. Sci. Eng.* **40**(8), 1–18 (2018). <https://doi.org/10.1007/s40430-018-1318-y>
  34. Ilani, M.A., Khoshnevisan, M.: Powder mixed-electrical discharge machining (EDM) with the electrode is made by fused deposition modeling (FDM) at Ti–6Al–4V machining procedure. *Multisc. Multidiscip. Model. Exp. Des.* **3**, 173–186 (2020). <https://doi.org/10.1007/s41939-020-00070-6>
  35. Ilani, M.A., Khoshnevisan, M.: Mathematical and physical modeling of FE-SEM surface quality surrounded by the plasma channel

- within Al powder-mixed electrical discharge machining of Ti-6Al-4V. *Int. J. Adv. Manuf. Technol.* **112**, 3263–3277 (2021). <https://doi.org/10.1007/s00170-021-06626-1>
36. Taherkhani, A., Ilani, M.A., Ebrahimi, F., Huu, P.N., Long, B.T., Van Dong, P., Tam, N.C., Minh, N.D., Van Duc, N.: Investigation of surface quality in cost of goods manufactured (COGM) method of  $\mu$ -Al<sub>2</sub>O<sub>3</sub> powder-mixed-EDM process on machining of Ti-6Al-4V. *Int. J. Adv. Manuf. Technol.* **116**(5–6), 1783–1799 (2021). <https://doi.org/10.1007/s00170-021-07573-7>
  37. Ilani, M.A., Khoshnevisan, M.: Study of surfactant effects on intermolecular forces (IMF) in powder-mixed electrical discharge machining (EDM) of Ti-6Al-4V. *Int. J. Adv. Manuf. Technol.* **116**(5–6), 1763–1782 (2021). <https://doi.org/10.1007/s00170-021-07569-3>
  38. Ilani, M.A., Khoshnevisan, M.: An evaluation of the surface integrity and corrosion behavior of Ti-6Al-4 V processed thermodynamically by PM-EDM criteria. *Int. J. Adv. Manuf. Technol.* **120**(7–8), 5117–5129 (2022). <https://doi.org/10.1007/s00170-022-09093-4>
  39. Phan, N.H., Pi, V.N., Tuan, N.Q., Shirguppikar, S., Patil, M.S., Ilani, M.A., Hung, L.X., Muthuramalingam, T., Hung, T.Q.: Tool wear rate analysis of uncoated and AlCrNi coated aluminum electrode in EDM for Ti-6Al-4 V titanium alloy. In: *Advances in Engineering Research and Application Proceedings of the International Conference on Engineering Research and Applications*, pp 832–838. Springer: Heidelberg (2021)
  40. Phan, N.H., Pi, V.N., Shirguppikar, S., Patil, M.S., Ilani, M.A., Hung, L.X., Muthuramalingam, T., Hung, T.Q.: Material removal rate in electric discharge machining with aluminum tool electrode for Ti-6Al-4V titanium alloy. In: *Advances in Engineering Research and Application: Proceedings of the International Conference on Engineering Research and Applications*, pp 527–533. Springer: Heidelberg (2021)
  41. Mahdavijad, R.A., Ilani, M.A.: Superior advance research in the electro-discharge machining of Ti alloys. *Int. J. Sci. Res. Mech. Mater. Eng.* **3**, 19–38 (2019)
  42. Boopathi, S.: An investigation on gas emission concentration and relative emission rate of the near-dry wire-cut electrical discharge machining process. *Environ. Sci. Pollut. Res.* **29**(57), 86237–86246 (2022). <https://doi.org/10.1007/s11356-021-17658-1>
  43. Gowri, N.V., Dwivedi, J.N., Krishnaveni, K., Boopathi, S., Palaniappan, M., Medikondur, N.R.: Experimental investigation and multi-objective optimization of eco-friendly near-dry electrical discharge machining of shape memory alloy using Cu/SiC/Gr composite electrode. *Environ. Sci. Pollut. Res.* **2023**, 1–19 (2023). <https://doi.org/10.1007/s11356-023-26983-6>
  44. Boopathi, S., Alqahtani, A.S., Mubarakali, A., Panchatcharam, P.: Sustainable developments in near-dry electrical discharge machining process using sunflower oil-mist dielectric fluid. *Environ. Sci. Pollut. Res.* **2023**, 1–20 (2023). <https://doi.org/10.1007/s11356-023-27494-0>
  45. Xie, W., Guo, C., Wang, X. and Zhang, J.: Experimental comparative study on Near-dry wire-cut electrical discharge machining process using moistened wire. (2023). <https://doi.org/10.21203/rs.3.rs-2612583/v1>
  46. Kuo, C.G., Hsu, C.Y., Chen, J.H., Lee, P.W.: Discharge current effect on machining characteristics and mechanical properties of aluminum alloy 6061 workpiece produced by electric discharging machining process. *Adv. Mech. Eng.* **9**(11), 1687814017730756 (2017). <https://doi.org/10.1177/1687814017730756>
  47. Montgomery, D.C., Myers, R.H.: *Process and product optimization using designed experiments*. Wiley, New York (2002)
  48. Box, G.E., Hunter, J.S., Hunter, W.G.: *Statistics for experimenters. Wiley series in probability and statistics*. Wiley, New York (2005)
  49. Montgomery, D.C.: *Design and analysis of experiments*. Wiley, New York (2006)
  50. Heinze, G., Dunkler, D.: Five myths about variable selection. *Transpl. Int.* **30**, 6–10 (2017). <https://doi.org/10.1111/tri.12895>
  51. Mishra, Y.K., Mishra, S., Jaiswal, S.C.: Comparative analysis of grey relational analysis integrated with the principal component analysis and analytic hierarchy process for multi-objective optimization of inclined laser percussion drilling in carbon fiber reinforced composites. *J. Adv. Manuf. Syst.* **21**(1), 1–23 (2022). <https://doi.org/10.1142/S0219686721500475>
  52. Mishra, Y.K., Mishra, S., Jaiswal, S.C.: Parametric analysis and optimization of inclined laser percussion drilling of carbon fiber reinforced plastic using solid state Nd: YAG laser. *Lasers Manuf. Mater. Process.* **8**, 325–354 (2021). <https://doi.org/10.1007/s40516-021-00151-5>
  53. Singh, D.P., Mishra, S., Porwal, R.K.: Parametric analysis through ANFIS modelling and optimization of micro-hole machining in super duplex stainless steel by die-sinking EDM. *Adv. Mater. Process. Technol.* (2022). <https://doi.org/10.1080/2374068X.2022.2135733>
  54. Ezeddini, S., Boujelbene, M., Bayraktar, E., Ben Salem, S.: Optimization of the surface roughness parameters of Ti–Al intermetallic based composite machined by wire electrical discharge machining. *Coatings* **10**(9), 900 (2020). <https://doi.org/10.3390/coatings10090900>

**Publisher's Note** Springer Nature remains neutral with regard to jurisdictional claims in published maps and institutional affiliations.

Springer Nature or its licensor (e.g. a society or other partner) holds exclusive rights to this article under a publishing agreement with the author(s) or other rightsholder(s); author self-archiving of the accepted manuscript version of this article is solely governed by the terms of such publishing agreement and applicable law.